# Supplementary Material

## A consensus estimate for the ice thickness distribution of all glaciers on Earth

Daniel Farinotti[1,2], Matthias Huss[1,3], Johannes J. Fürst[4], Johannes Landmann[1,2], Horst Machguth[3,5], Fabien Maussion[6], and Ankur Pandit[7]

[1] Laboratory of Hydraulics, Hydrology and Glaciology (VAW), ETH Zurich, Zurich, Switzerland
[2] Swiss Federal Institute for Forest, Snow and Landscape Research (WSL), Birmensdorf, Switzerland
[3] Department of Geosciences, University of Fribourg, Fribourg, Switzerland
[4] Inst. of Geography, Friedrich-Alexander-University Erlangen-Nuremberg (FAU), Erlangen, Germany
[5] Department of Geography, University of Zurich, Zurich, Switzerland
[6] Institute of Atmospheric and Cryospheric Sciences, University of Innsbruck, Innsbruck, Austria
[7] Interdisciplinary Programme in Climate Studies, Indian Institute of Technology, Bombay, India

# S 1 Setup of individual models

The models used within the study have been presented in earlier publications (Huss and Farinotti, 2012; Frey et al., 2014; Fürst et al., 2017; Ramsankaran et al., 2018; Maussion et al., 2018) and are summarized in Farinotti et al. (2017). This section mainly provides additional implementation-details used for the present work.

## S 1.1 Model 1 (*HF-model*) – Huss and Farinotti (2012)

The *HF-model* by Huss and Farinotti (2012) is based on mass conservation and principles of ice flow dynamics. Basically, the approach estimates the ice volume flux along the glacier, and converts it into ice thickness by using Glen's flow law (Glen, 1955). Glacier hypsometry and surface characteristics (mean slope and glacier width) are evaluated for 10 m elevation bands, and all calculations are performed with this simplified two dimensional shape. Apparent mass balance gradients for the ablation and accumulation area (Farinotti et al., 2009) are estimated based on the continentality of the glacier. Ice volume fluxes along the glacier are converted into ice thickness using an integrated form of Glen's flow law. Longitudinal variations in valley shape and basal shear stress are taken into account. Simple parametrisations describe both the temperature-dependence of the flow rate factor and the variability in basal sliding. Calculated mean elevation-band thickness is extrapolated to each cell of a regular grid considering local surface slope, and the distance from the glacier margin. For marine-terminating glaciers, a fixed ice volume flux is prescribed at the glacier terminus.

For the here presented results, the model was calibrated to the available ice thickness measurements by optimizing parameters specific to each RGI region. No model tuning was performed to reproduce ice thickness observations of individual glaciers. The misfit with observations was assessed by evaluating (i) the region-by-region average of the mean deviations of all points of individual glaciers, (ii) the glacier-area-weighted average of the mean deviation over all points of individual glaciers, (iii) the average of the difference between calculated and reported mean ice thickness, and (iv) the glacier-area-weighted average of the difference between calculated and reported mean ice thickness. Original model parameters used in Huss and Farinotti (2012) were adjusted to minimize each of the criteria (i) to (iv), with the aim of minimizing systematic deviations from the observations. For roughly half of the regions, no re-calibration was necessary. For the remaining RGI regions, the apparent mass balance gradient $d\widetilde{b}/dz$ (see Equation 1 in Huss and Farinotti, 2012) was adjusted within physically reasonable bounds. For two RGI regions, also the flow rate factor $A_f$ (Equation 5 in Huss and Farinotti, 2012) was re-calibrated.

## S 1.2 Model 2 (*GlabTop2*) – Frey et al. (2014)

The *GlabTop2* model is based on the same concepts as presented in Linsbauer et al. (2012), and uses an empirical relation between average basal shear stress and glacier elevation range (Haeberli and Hoelzle, 1995) to calculate the ice thickness at individual locations. The laborious process of manually drawing branchlines, required in the original approach (Linsbauer et al., 2012), is avoided by determining the local surface slope from the average of all grid cells within a predefined elevation buffer. This makes the entirely grid-based method applicable to the large scale. In a first step, an ice thickness is calculated at a set of randomly selected cells. In a second step, this thickness is interpolated to the entire glacier area. To achieve realistic glacier cross-sections, the interpolation scheme assigns a minimum, non-zero ice thickness to all grid

cells directly adjacent to the glacier margin.
Parameter selection for the *GlabTop2* model was identical to the one described in Farinotti et al. (2017), with the exception of the shape factor $f$ (see Equation 3 in Frey et al., 2014). For the latter, an empirically derived function of the form $f = a \cdot (n_g/n_m)^b$ was used, where $n_g$ is the total number of grid cells of a glacier, $n_m$ is the number of glacier grid cells that are directly adjacent to the glacier margin, and $a$ and $b$ are two empirical coefficients. The additional constraint $f \leq 1$ was imposed. Coefficients of $a = 5596$ and $b = 0.1688$ were determined during the cross-validation experiment (see Methods in the main article) by minimizing the difference between (i) the average ice thickness given by the measurements and (ii) the average thickness given by the model at the corresponding locations (no calibration at the level of individual points was performed). Note that the dependency of $f$ on $r = n_g/n_m$ can be interpreted as the effect of the drag from valley walls on glacier flow (Paterson, 1994). For a given surface slope, a low $r$ value (typical for a valley-type glacier) results in a higher ice thickness than a high $r$ value (typical for ice caps). Values of $f$ were limited to $\leq 1$, thus varying from 0.5596 to 1.
For the ice thickness calculations, DEMs with a spatial resolution below 75 m were resampled to 75 m, and re-brought to the original resolution afterwards. This is to reduce the noise that is introduced when strong, small-scale variations in surface slope occur (such variations directly affect the calculated ice thickness through the dependence on surface slope; e.g. Frey et al., 2014; Farinotti et al., 2017). No thickness calculations were performed when (1) the provided surface DEM contained negative values for more than 5 % of the area, and (2) the estimated ice thickness was unrealistically high. To discern case (1), an arbitrary threshold of 100 m below sea level was used. If this threshold was reached by fewer than 5% of the DEM extent, the corresponding elevations were set to sea level (0 m a.s.l.); if the threshold was reached by more than 5% of the DEM extent, the glacier was not considered. To discern case (2), a threshold of 900 m ice thickness was set. In cases where the threshold was met by 20% or more of the glacier domain, the results were discarded. The number of so-excluded glaciers is very small (0.05 % of the total) but the glaciers represent a disproportionally large fraction of both the global glacier area (ca. 12 %) and volume (ca. 28 %).

### S 1.3 Model 3 (*OGGM*) – Maussion et al. (2018)

The *Open Global Glacier Model* (*OGGM*; Maussion et al., 2018) is an open-source model for glacier dynamics applicable on any glacier in the world. The ice thickness inversion scheme relies on a mass-conservation approach similar to that of Farinotti et al. (2009), but is fully automated. The ice thickness is computed from mass turnover and the shallow ice approximation along multiple flowlines computed with the algorithm of Kienholz et al. (2014). A major difference from other models is that OGGM relies on gridded climate data (CRU in this instance; Harris et al., 2014) to compute the mass turnover, and not on predefined linear gradients.
The OGGM parameter calibration for this study was limited to (i) the interpolation parameters used to translate the flowline thickness to a distributed ice thickness map, and (ii) the creep parameter $A$ in Glen's flow law (Glen, 1955). All other parameters are kept to their default values (see Maussion et al., 2018). The interpolation parameters were selected to minimize the glacier-wide root mean square deviation from actual ice thickness measurements, with $A$ chosen to minimize the glacier-wide bias. Once the interpolation step was fixed, Glen's $A$ was chosen to minimize the bias to all point observations in a given cross-validation set.
Unlike other models, OGGM does not rely on any regional tuning, i.e. the same set of parameters is used globally and for each cross-validation set. The reasoning behind this decision is that RGI regions are often arbitrary, and do not necessarily represent an homogeneous entity in terms

of climate or glaciological processes. Regional tuning might thus introduce artificial, model-dependant differences between regions that are not found in reality.
A subjective assessment of the main sources of uncertainty (not ordered by importance) are (1) the reliance on actual gridded climate data to estimate the mass-turnover, (2) the interpolation step required to transpose the flowline representation into a two dimensional one, (3) uncertainties in the actual ice dynamics parameters (deformation and sliding in particular), and (4) uncertainties in the location and detection of glacier ice-divides.

### S 1.4 Model 4 (no specific name so far)– Fürst et al. (2017)

The approach by Fürst et al. (2017) is primarily based on mass conservation and solves for a basin-wide thickness field. A detailed description and performance analysis for various glacier types on Svalbard was presented in the mentioned publication. The approach is split into two steps to ensure wide applicability. For the global application, only the first step was applicable since no surface velocities were available. Similar as for Models 1 and 3, this step relies on the shallow-ice approximation for a flux-thickness conversion. Point measurements of ice thickness are readily assimilated and reproduced by an automatic viscosity calibration.
The only adaptation concerns the ability to use information on mean glacier thickness (provided within the *Glacier Thickness Database*; WGMS, 2016). For this purpose, a glacier-wide uniform ice viscosity is calibrated such that the mean glacier thickness is reproduced. Information on surface mass balance (SMB) for each glacier is based on the results of the *Global Glacier Evolution Model* (*GloGEM*; Huss and Hock, 2015). The flowline SMB is averaged for the period 1980 – 2010. Values are extrapolated over the drainage basin following elevation bands. For marine terminating glaciers, surface elevation changes were set to zero. For land-terminating glaciers, elevation changes are parametrized by an empirical relations given in Huss et al. (2010), which distinguishes between three glacier area classes.

### S 1.5 Model 5 (*GlabTop2_IITB version*) – Ramsankaran et al. (2018)

The *GlabTop2_IITB version* (referred to as *RAAJglabtop2* in Farinotti et al., 2017) is an independent implementation of the *GlabTop2* model developed by Frey et al. (2014) (Model 2 above; cf. Sec. S 1.2).
Calibration of the model followed Ramsankaran et al. (2018). In a nutshell, the method's shape factor $f$ (see Equation 3 in Ramsankaran et al., 2018) is used as the only calibration parameter, and direct ice thickness observations are used to iteratively adjust $f$ so that the squared differences between modelled and observed ice thicknesses are minimized. Since no direct ice thickness estimates were available for the vast majority of the 1152 glaciers considered by the model, a set of 31 simulations were performed by varying $f$ in the interval $f = [0.6, 0.9]$ with a spacing of 0.01. The so-obtained ice thickness distributions where then stacked by averaging pixel-wise the local ice thickness obtained from the individual simulations. The so obtained distribution was used as the best estimate.

Table S 1: Weights assigned to individual models (M1 to M5). Values are derived with the cross-validation experiment described in the Methods section of the main text. $N_{\mathrm{meas}}$ is the number of glaciers for which ice thickness information is reported within GlaThiDa v2. For regions with $N_{\mathrm{meas}} < 5$ (labelled with *), the weights are obtained by pooling all regions. Weights are relative, and are distributed amongst models that actually provide a solution for a given region (i.e. the sum of the weights is 100 % for every region).

| RGI region | | $N_{\mathrm{meas}}$ | M1 | M2 | M3 | M4 | M5 |
|---|---|---|---|---|---|---|---|
| 01 | Alaska | 9 | 45 % | 22 % | 33 % | - | - |
| 02 | Western Canada and US | 29 | 35 % | 29 % | 35 % | - | - |
| 03 | Arctic Canada North | 235 | 35 % | 30 % | 35 % | - | - |
| 04 | Arctic Canada South | 24 | 27 % | 32 % | 40 % | - | - |
| 05 | Greenland Periphery | 204 | 44 % | 56 % | - | - | - |
| 06 | Iceland | 3* | 38 % | 32 % | 30 % | - | - |
| 07 | Svalbard [(1)] | 65 | - | - | - | (100 %) | - |
| 08 | Scandinavia | 97 | 26 % | 19 % | 25 % | 31 % | - |
| 09 | Russian Arctic | 15 | 30 % | 33 % | 37 % | - | - |
| 10 | North Asia | 20 | 25 % | 39 % | 36 % | - | - |
| 11 | Central Europe | 125 | 27 % | 27 % | 12 % | 15 % | 18 % |
| 12 | Caucasus and Middle East | 21 | 31 % | 25 % | 23 % | - | 21 % |
| 13 | Central Asia | 38 | 25 % | 25 % | 20 % | 31 % | - |
| 14 | South Asia West | 0* | 31 % | 26 % | 25 % | - | 18 % |
| 15 | South Asia East | 2* | 26 % | 22 % | 20 % | 32 % | - |
| 16 | Low Latitudes | 4* | 38 % | 32 % | 30 % | - | - |
| 17 | Southern Andes | 38 | 41 % | 42 % | 17 % | - | - |
| 18 | New Zealand | 2* | 26 % | 22 % | 20 % | 32 % | - |
| 19 | Antarctic and Subantarctic | 69 | 60 % | 40 % | - | - | - |
| All regions pooled | | 1000 | 22 % | 19 % | 18 % | 28 % | 13 % |

[(1)] For Svalbard, estimates are taken from Fürst et al. (2018), who used a method similar to M 4 (Fürst et al., 2017).

## Same weight for every region

Table S 2: Estimated regional glacier ice volumes from this and previous studies. Values are given in mm sea level equivalent (see Methods in the main text). Numbers for this study (a) refer to the composite solution, (b) do not correct for ice portions below present sea level (in line with previous studies but contrary to Table 1 of the main text), and (c) are obtained by assigning the same, pooled weight (see last row of Table S 1) to every RGI region. When previous studies used a different regions nomenclature, correspondence is given in the table's footnotes.

| RGI region | This study | Radić and Hock (2010)[1] | Huss and Farinotti (2012) | Marzeion et al. (2012) | Grinsted (2013) | Radić et al. (2014) | Frey et al. (2014)[4] | Martín-Español et al. (2015) | Average of previous estimates | Difference between this study and average of previous estimates | Difference between this study and Huss and Farinotti (2012) |
|---|---|---|---|---|---|---|---|---|---|---|---|
| 01 Alaska | 45.8 | 66.3 | 49.3 | 75.1 | 43.3 | 67.3 | - | - | 60.3 | (-23.9 %) | [ -7.0 %] |
| 02 Western Canada and US | 2.6 | 4.6 | 2.5 | 3.0 | 2.5 | 3.1 | - | - | 3.1 | (-18.7 %) | [ 2.9 %] |
| 03 Arctic Canada North | 68.4 | 193.6 | 83.1 | 100.6 | 59.9 | 134.1 | - | - | 114.3 | (-40.1 %) | [-17.6 %] |
| 04 Arctic Canada South | 20.8 | -[2] | 23.7 | 20.2 | 14.8 | 22.6 | - | - | 20.3 | ( 2.4 %) | [-12.3 %] |
| 05 Greenland Periphery | 37.9 | 43.1 | 46.0 | 26.8 | 45.7 | 41.4 | - | - | 40.6 | ( -6.6 %) | [-17.6 %] |
| 06 Iceland | 9.1 | 11.8 | 10.7 | 12.4 | 8.5 | 6.4 | - | - | 10.0 | ( -8.7 %) | [-15.1 %] |
| 07 Svalbard | 18.0 | 24.8 | 23.4 | 21.5 | 12.9 | 22.0 | - | 16.2 | 20.1 | (-10.3 %) | [-22.9 %] |
| 08 Scandinavia | 0.7 | 0.5 | 0.6 | 0.6 | 0.8 | 0.5 | - | - | 0.6 | ( 20.2 %) | [ 16.4 %] |
| 09 Russian Arctic | 35.4 | 42.8 | 40.7 | 57.1 | 32.8 | 42.9 | - | - | 43.3 | (-18.3 %) | [-13.1 %] |
| 10 North Asia | 0.3 | 0.4 | 0.3 | 0.6 | 0.5 | 0.7 | - | - | 0.5 | (-34.1 %) | [ -3.6 %] |
| 11 Central Europe | 0.3 | 0.5 | 0.3 | 0.3 | 0.3 | 0.3 | - | - | 0.3 | ( -8.0 %) | [ 8.5 %] |
| 12 Caucasus and Middle East | 0.2 | 0.2 | 0.1 | 0.2 | 0.2 | 0.2 | - | - | 0.2 | (-16.0 %) | [ 3.3 %] |
| 13 Central Asia | 7.9 | 30.1 | 12.1 | 15.2 | 23.0 | 15.7 | - | - | 19.2 | (-58.9 %) | [-34.9 %] |
| 14 South Asia West | 6.9 | -[3] | 7.8 | 9.2 | 9.2 | 10.8 | 6.8 | - | 8.8 | (-21.2 %) | [-11.6 %] |
| 15 South Asia East | 2.1 | -[3] | 3.2 | 3.7 | 4.0 | 4.5 | 2.2 | - | 3.5 | (-39.4 %) | [-33.2 %] |
| 16 Low Latitudes | 0.2 | 0.8 | 0.3 | 0.6 | 0.3 | 0.6 | - | - | 0.5 | (-54.6 %) | [-31.9 %] |
| 17 Southern Andes | 12.9 | 19.6 | 16.1 | 12.4 | 11.4 | 16.5 | - | - | 15.2 | (-15.2 %) | [-20.0 %] |
| 18 New Zealand | 0.2 | 0.2 | 0.2 | 0.2 | 0.3 | 0.2 | - | - | 0.2 | (-15.1 %) | [ 4.3 %] |
| 19 Antarctic and Subantarctic | 112.2 | 143.8 | 90.6 | - | 73.0 | 117.5 | - | - | 106.2 | ( 5.7 %) | [ 23.9 %] |
| TOTAL | 381.9 | 583.1 | 411.0 | 359.7 | 343.4 | 507.3 | - | - | 467.2 | (-18.2 %) | [ -7.1 %] |
| Arctic (03+04+05+07+09) | 180.5 | 304.3 | 216.9 | 226.2 | 166.1 | 263.0 | - | - | 238.6 | (-24.4 %) | [-16.8 %] |
| Antarctic (19) | 112.2 | 143.8 | 90.6 | - | 73.0 | 117.5 | - | - | 106.2 | ( 5.6 %) | [ 23.8 %] |
| Alaska (01) | 45.8 | 66.3 | 49.3 | 75.1 | 43.3 | 67.3 | - | - | 60.3 | (-24.0 %) | [ -7.1 %] |
| High Mountain Asia (13+14+15) | 16.9 | 30.1 | 23.1 | 28.1 | 36.2 | 31.0 | - | - | 31.5 | (-46.3 %) | [-26.8 %] |
| Other (9 regions) | 26.5 | 38.6 | 31.1 | 30.3 | 24.8 | 28.5 | - | - | 30.6 | (-13.4 %) | [-14.8 %] |

[1] Regions nomenclature: RGI region (Reg.) 10 = Franz Josef Land + Novaya Zemlya + Severnaya Zemlya; Reg. 16 = South America I; Reg. 17 = South America II; Reg. 19 = Sub-Antarctic islands + Antarctica

[2] Volume accounted for within Reg. 04.

[3] Volume accounted for within Reg. 13.

[4] Regions nomenclature: Reg. 14 = Karakoram + West Himalayas; Reg. 15 = Central Himalayas + East Himalayas

# Regionally differentiated weights

Table S 3: Same as Table S 2, but for the case in which regionally differentiated weights (see Table S 1) are assigned to individual models.

| RGI region | This study | Radić and Hock (2010)[1] | Huss and Farinotti (2012) | Marzeion et al. (2012) | Grinsted (2013) | Radić et al. (2014) | Frey et al. (2014)[4] | Martín-Español et al. (2015) | Average of previous estimates | Difference between this study and average of previous estimates | Difference between this study and Huss and Farinotti (2012) |
|---|---|---|---|---|---|---|---|---|---|---|---|
| 01 Alaska | 45.5 | 66.3 | 49.3 | 75.1 | 43.3 | 67.3 | - | - | 60.3 | (-24.4 %) | [ -7.6 %] |
| 02 Western Canada and US | 2.6 | 4.6 | 2.5 | 3.0 | 2.5 | 3.1 | - | - | 3.1 | (-18.2 %) | [ 3.5 %] |
| 03 Arctic Canada North | 68.0 | 193.6 | 83.1 | 100.6 | 59.9 | 134.1 | - | - | 114.3 | (-40.5 %) | [-18.1 %] |
| 04 Arctic Canada South | 20.4 | -[2] | 23.7 | 20.2 | 14.8 | 22.6 | - | - | 20.3 | ( 0.6 %) | [-13.8 %] |
| 05 Greenland Periphery | 37.8 | 43.1 | 46.0 | 26.8 | 45.7 | 41.4 | - | - | 40.6 | ( -6.8 %) | [-17.7 %] |
| 06 Iceland | 9.1 | 11.8 | 10.7 | 12.4 | 8.5 | 6.4 | - | - | 10.0 | ( -8.6 %) | [-15.1 %] |
| 07 Svalbard | 18.0 | 24.8 | 23.4 | 21.5 | 12.9 | 22.0 | - | 16.2 | 20.1 | (-10.3 %) | [-22.9 %] |
| 08 Scandinavia | 0.7 | 0.5 | 0.6 | 0.6 | 0.8 | 0.5 | - | - | 0.6 | ( 21.4 %) | [ 17.6 %] |
| 09 Russian Arctic | 35.0 | 42.8 | 40.7 | 57.1 | 32.8 | 42.9 | - | - | 43.3 | (-19.1 %) | [-14.0 %] |
| 10 North Asia | 0.3 | 0.4 | 0.3 | 0.6 | 0.5 | 0.7 | - | - | 0.5 | (-34.6 %) | [ -4.3 %] |
| 11 Central Europe | 0.3 | 0.5 | 0.3 | 0.3 | 0.3 | 0.3 | - | - | 0.3 | (-10.1 %) | [ 6.0 %] |
| 12 Caucasus and Middle East | 0.2 | 0.2 | 0.1 | 0.2 | 0.2 | 0.2 | - | - | 0.2 | (-17.3 %) | [ 1.6 %] |
| 13 Central Asia | 7.8 | 30.1 | 12.1 | 15.2 | 23.0 | 15.7 | - | - | 19.2 | (-59.2 %) | [-35.4 %] |
| 14 South Asia West | 6.9 | -[3] | 7.8 | 9.2 | 9.2 | 10.8 | 6.8 | - | 8.8 | (-21.3 %) | [-11.8 %] |
| 15 South Asia East | 2.1 | -[3] | 3.2 | 3.7 | 4.0 | 4.5 | 2.2 | - | 3.5 | (-39.8 %) | [-33.6 %] |
| 16 Low Latitudes | 0.2 | 0.8 | 0.3 | 0.6 | 0.3 | 0.6 | - | - | 0.5 | (-54.6 %) | [-31.9 %] |
| 17 Southern Andes | 12.9 | 19.6 | 16.1 | 12.4 | 11.4 | 16.5 | - | - | 15.2 | (-15.0 %) | [-19.8 %] |
| 18 New Zealand | 0.2 | 0.2 | 0.2 | 0.2 | 0.3 | 0.2 | - | - | 0.2 | (-12.8 %) | [ 7.1 %] |
| 19 Antarctic and Subantarctic | 112.3 | 143.8 | 90.6 | - | 73.0 | 117.5 | - | - | 106.2 | ( 5.8 %) | [ 24.0 %] |
| TOTAL | 380.3 | 583.1 | 411.0 | 359.7 | 343.4 | 507.3 | - | - | 467.2 | (-18.5 %) | [ -7.4 %] |
| Arctic (03+04+05+07+09) | 179.2 | 304.3 | 216.9 | 226.2 | 166.1 | 263.0 | - | - | 238.6 | (-24.9 %) | [-17.4 %] |
| Antarctic (19) | 112.3 | 143.8 | 90.6 | - | 73.0 | 117.5 | - | - | 106.2 | ( 5.7 %) | [ 24.0 %] |
| Alaska (01) | 45.5 | 66.3 | 49.3 | 75.1 | 43.3 | 67.3 | - | - | 60.3 | (-24.5 %) | [ -7.7 %] |
| High Mountain Asia (13+14+15) | 16.8 | 30.1 | 23.1 | 28.1 | 36.2 | 31.0 | - | - | 31.5 | (-46.7 %) | [-27.3 %] |
| Other (9 regions) | 26.5 | 38.6 | 31.1 | 30.3 | 24.8 | 28.5 | - | - | 30.6 | (-13.4 %) | [-14.8 %] |

[1] Regions nomenclature: RGI region (Reg.) 10 = Franz Josef Land + Novaya Zemlya + Severnaya Zemlya; Reg. 16 = South America I; Reg. 17 = South America II; Reg. 19 = Sub-Antarctic islands + Antarctica

[2] Volume accounted for within Reg. 04.

[3] Volume accounted for within Reg. 13.

[4] Regions nomenclature: Reg. 14 = Karakoram + West Himalayas; Reg. 15 = Central Himalayas + East Himalayas

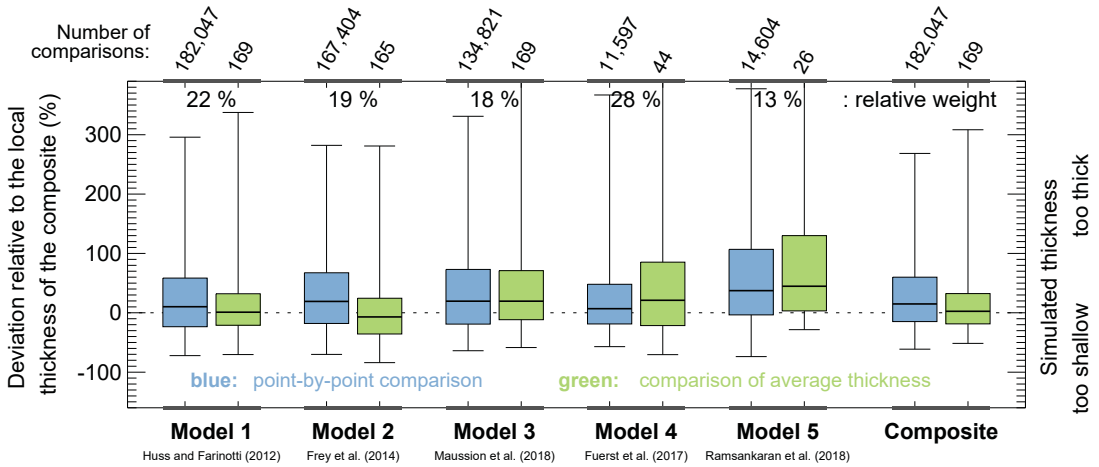


Figure S 1: Assessment of model performance. The distribution of the relative deviations between modelled and measured ice thickness is shown for every model and for the composite solution. Deviations are given relative to the ice thickness of the composite and refer to point-by-point comparisons (blue) or comparisons of the average thickness (green). The number of points composing each box plot is given above the plot. Box plots show the 95% confidence interval (whiskers), the interquartile range (box), and the median (lines within box). "Relative weight" refers to the weight assigned to individual models when producing the composite solution (cf. Methods in the main text and Table S 1).

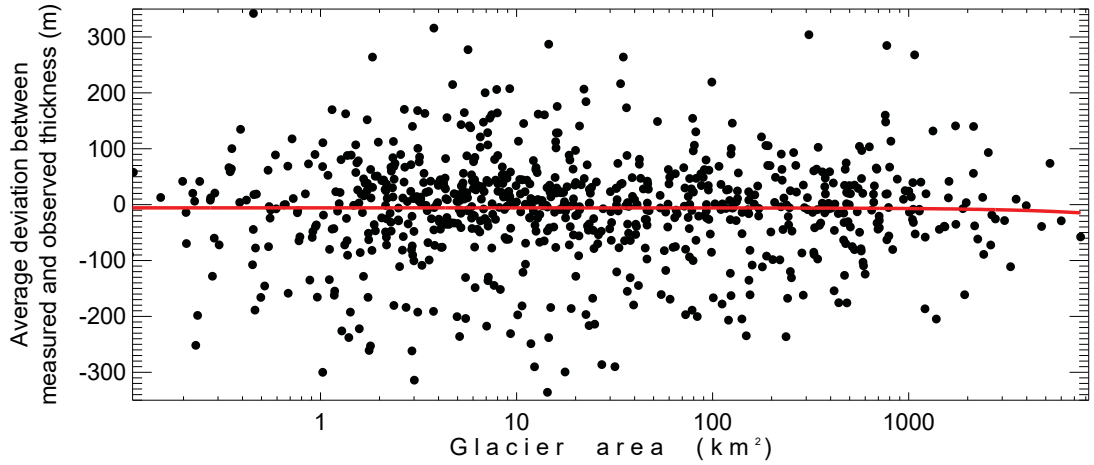


Figure S 2: Assessment of possible bias in the results. The mean deviation between measured and observed ice thickness is shown as a function of glacier size. The red line is a linear fit through all points, and shows no discernible trend. Note the logarithmic scale for glacier area.

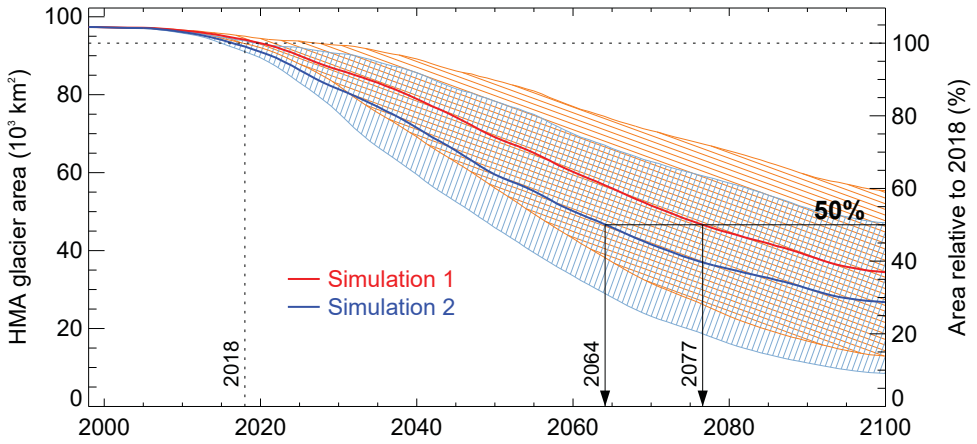


Figure S 3: Implication of the estimated present-day ice thickness on the projected glacier area evolution for High Mountain Asia (RGI regions 13+14+15). Projections are based on the Global Glacier Evolution Model (GloGEM; see Huss and Hock, 2015, and "Methods" section of the main text), which was forced with the output of 14 different climate models under Representative Concentration Pathway 4.5 (Meinshausen et al., 2011). Simulation 1 and 2 are based on the ice thickness distribution presented by Huss and Farinotti (2012) and this study, respectively. Thick lines represent the ensemble median, whilst the bands are 95 % confidence intervals. The time by which 50 % of the present-day (year 2018) glacier area has shrunk by 50 % is marked.

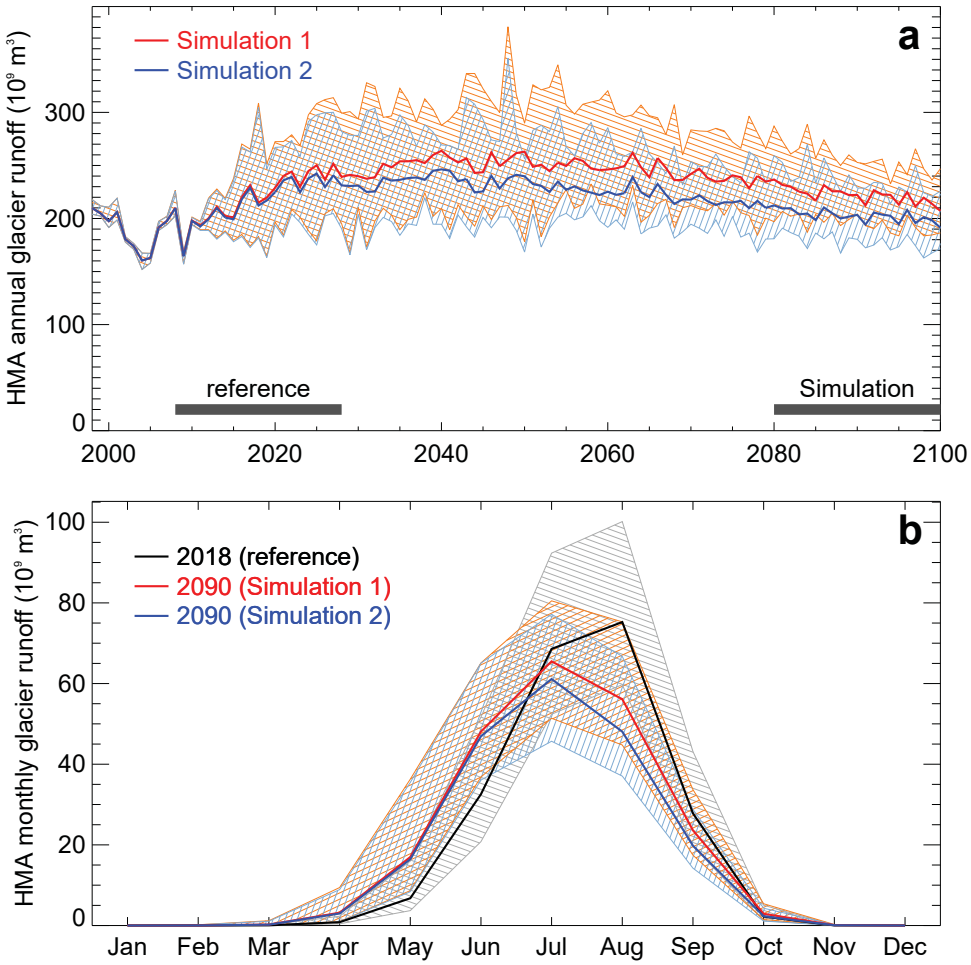


Figure S 4: Implication of the estimated present-day ice thickness on the projected glacier runoff evolution for High Mountain Asia (RGI regions 13+14+15). (a) Total annual glacier runoff. (b) Monthly glacier runoff averaged over a 20-year period around the indicated year (see also horizontal bars in panel a). Projections are based on the Global Glacier Evolution Model (GloGEM; see Huss and Hock, 2015, and "Methods" section of the main text), which was forced with the output of 14 different climate models under Representative Concentration Pathway 4.5 (Meinshausen et al., 2011). Simulation 1 and 2 are based on the ice thickness distribution presented by Huss and Farinotti (2012) and this study, respectively. Thick lines represent the ensemble median, whilst the bands are 95 % confidence intervals.

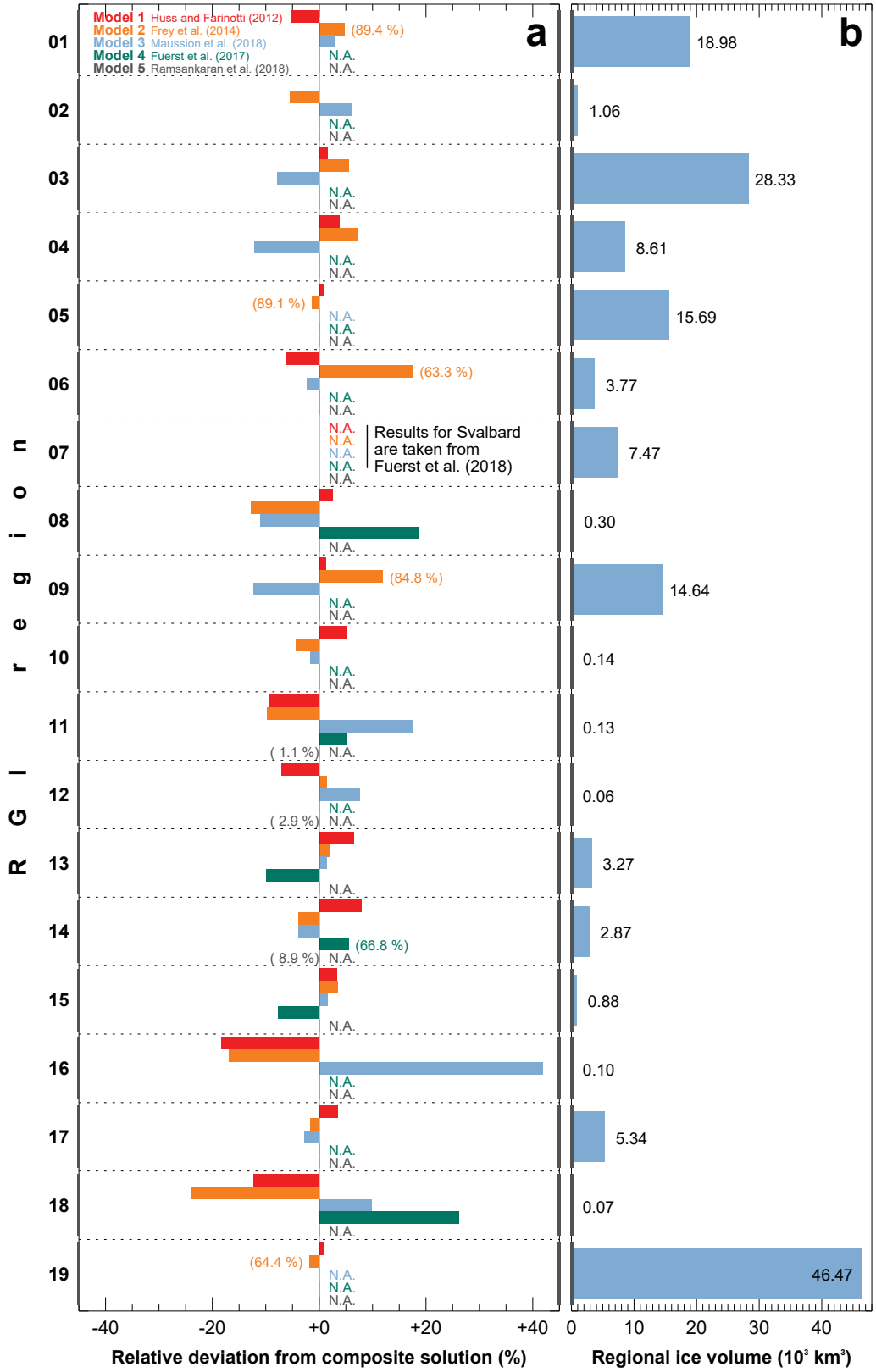


Figure S 5: (a) Difference with respect to the composite solution of the ice volume estimated by individual models for the 19 regions of the Randolph Glacier Inventory (RGI). The difference is only shown if the corresponding model considered at least 50 % of the regional glacier area (cf. Fig. 1a in the main text), and only refers to the portion of area actually considered (given within parenthesis if <95 %). (b) Total ice volume as estimated by the composite solution.

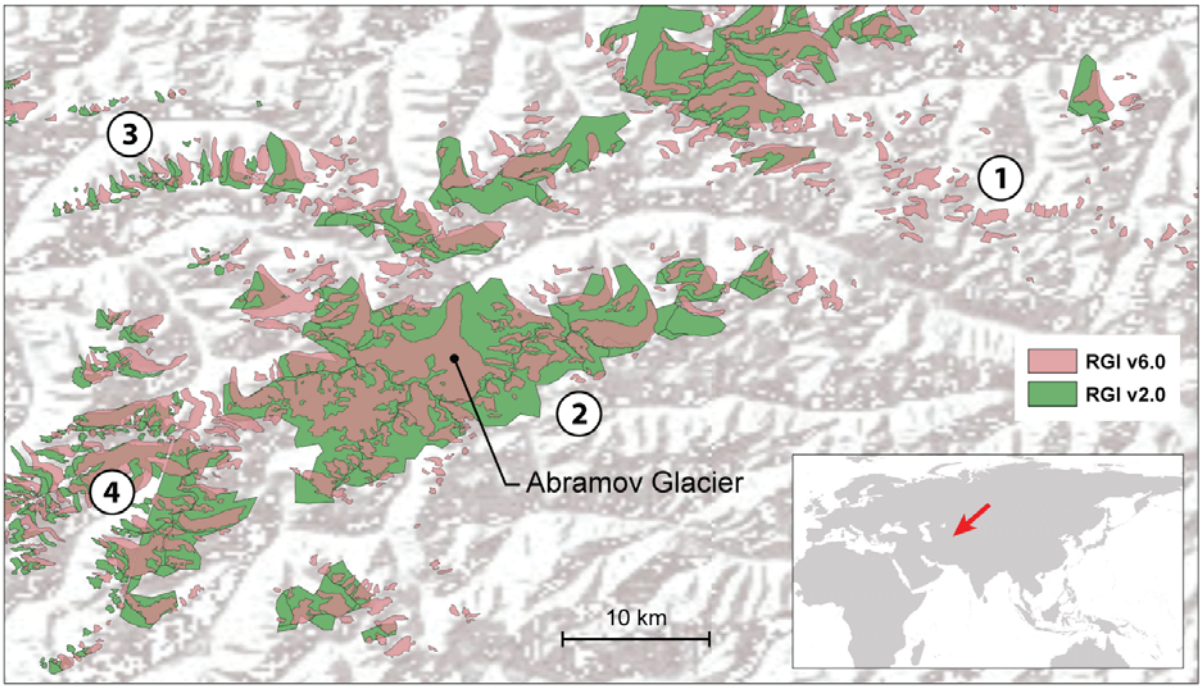


Figure S 6: Example for glacier outline changes between RGI version 2.0 (used by Huss and Farinotti, 2012) and RGI version 6.0 (used in this study). The example refers to the region of Abramov Glacier (labeled), Central Asia. The circled numbers highlight regions for which (1) previously missing glaciers are now inventoried, (2) glacier complexes have been subdivided, (3) geolocation was improved, and (4) artifacts were corrected.

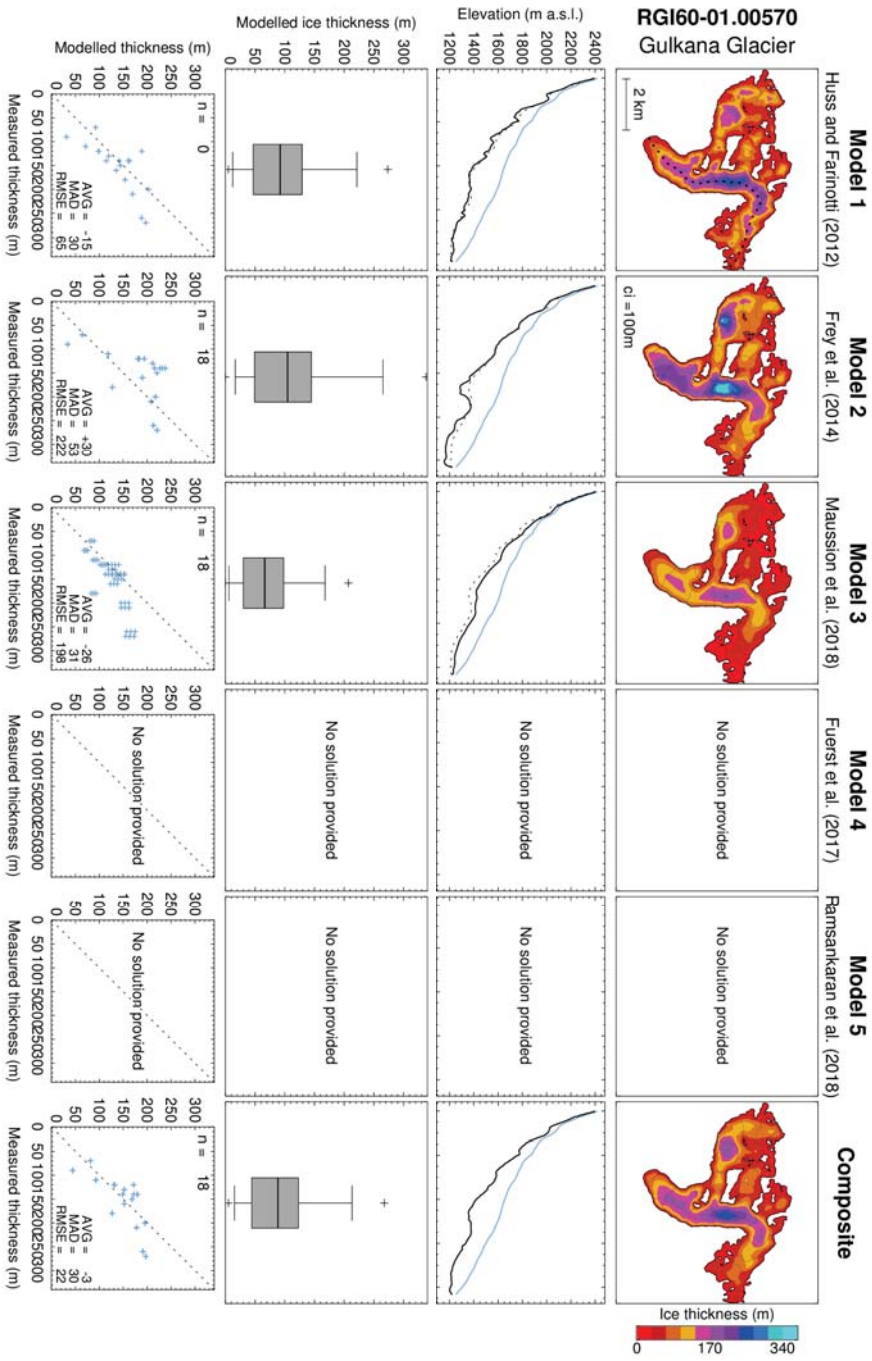


Figure S 7: Example for the estimated ice thickness distribution. The example is arbitrary, and refers to glacier RGI60-01.00570 (RGI region "Alaska"). Rows show the following: (1) Ice thickness distribution as estimated by the various models (Model 1 to 5), and the composite. Contour lines refer to surface topography (the contour interval *ci* is given in the second panel). (2) Longitudinal profile of the glacier surface (blue) and the estimated bedrock topography (solid black). The composite solution (dashed black) is given as a reference. The profile's location is shown in the first panel of the first row (dashed line). (3) Distribution of the estimated ice thickness. Boxplots show minimum and maximum values (crosses), 95% confidence intervals (whiskers), interquartile ranges (box), and medians (line within box). The mean ice thickness reported in GlaThiDa v2.0 (WGMS, 2016) is given when available (asterisk). (4) Scatter-plot between measured and modelled point (blue markers) and mean (asterisk) ice thickness. The following information is given: number of point measurements ($n$), average deviation ($AVG$), mean absolute deviation ($MAD$), root mean square error ($RMSE$). The scatter-plots show pooled data from the cross-validation experiment (see Methods in the main text). All other panels show the final solution.

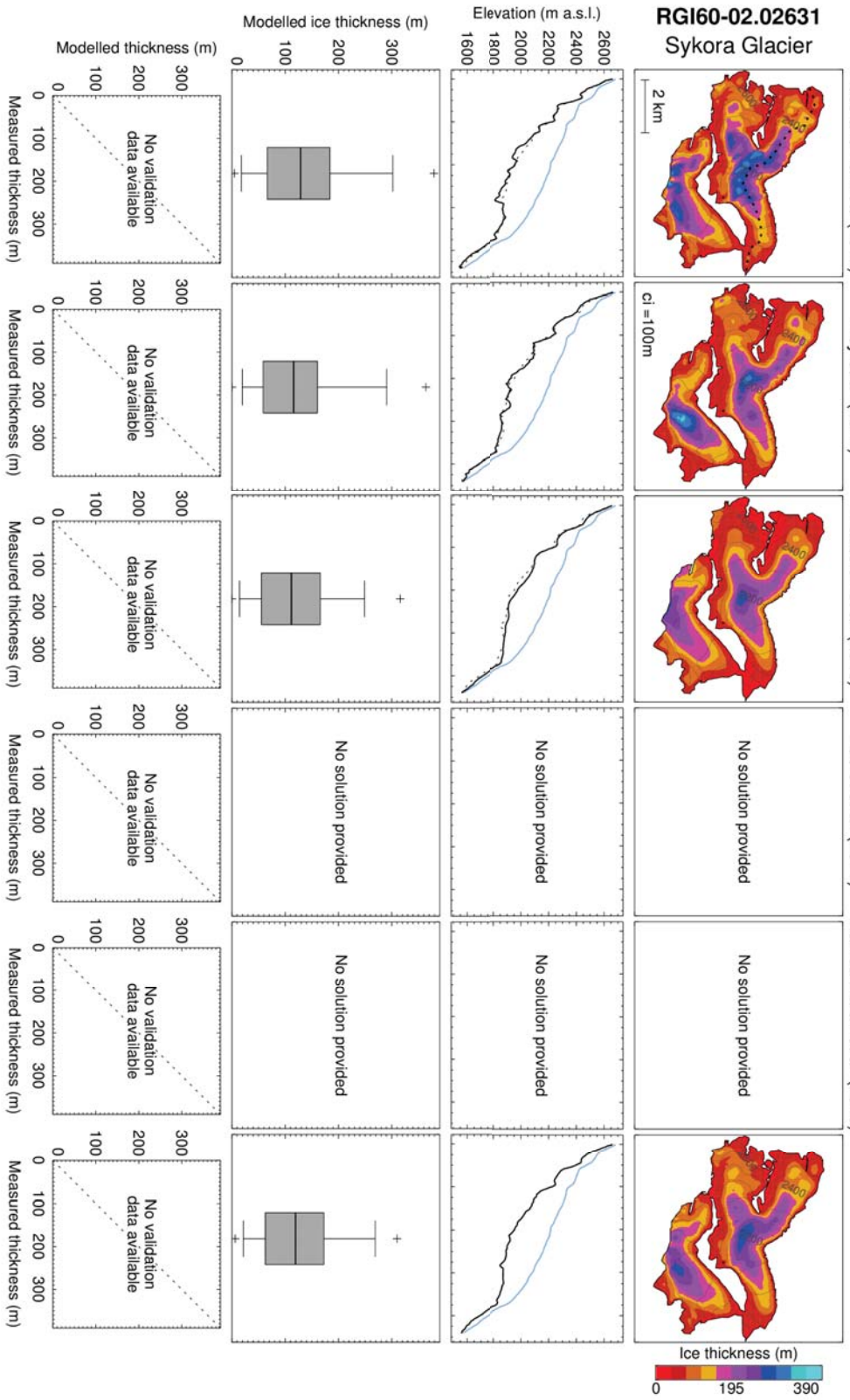


Figure S 8: Same as Figure S 7 but for glacier RGI60-02.02631 (RGI region "Western Canada and US").

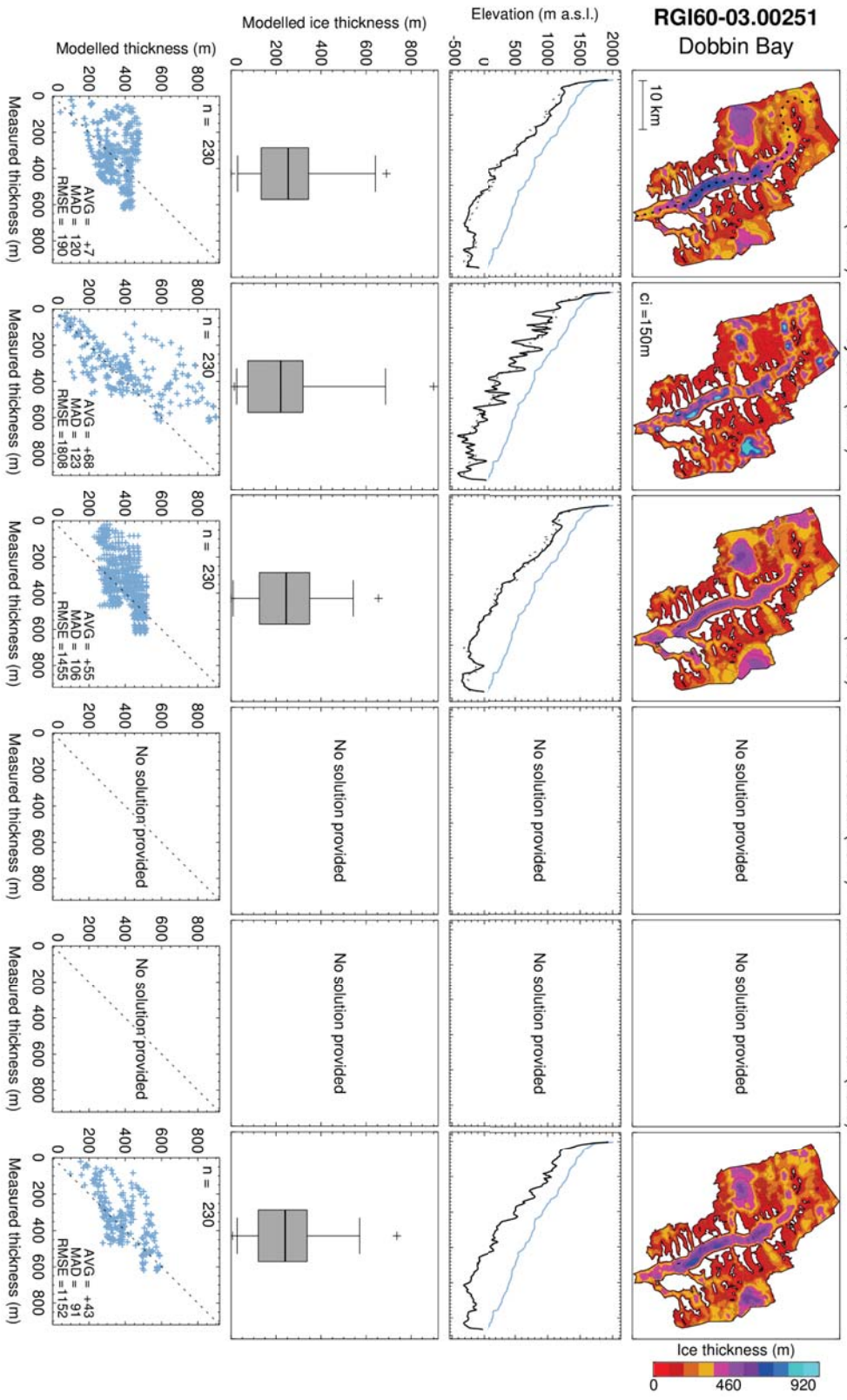


Figure S 9: Same as Figure S 7 but for glacier RGI60-03.00251 (RGI region "Arctic Canada North").

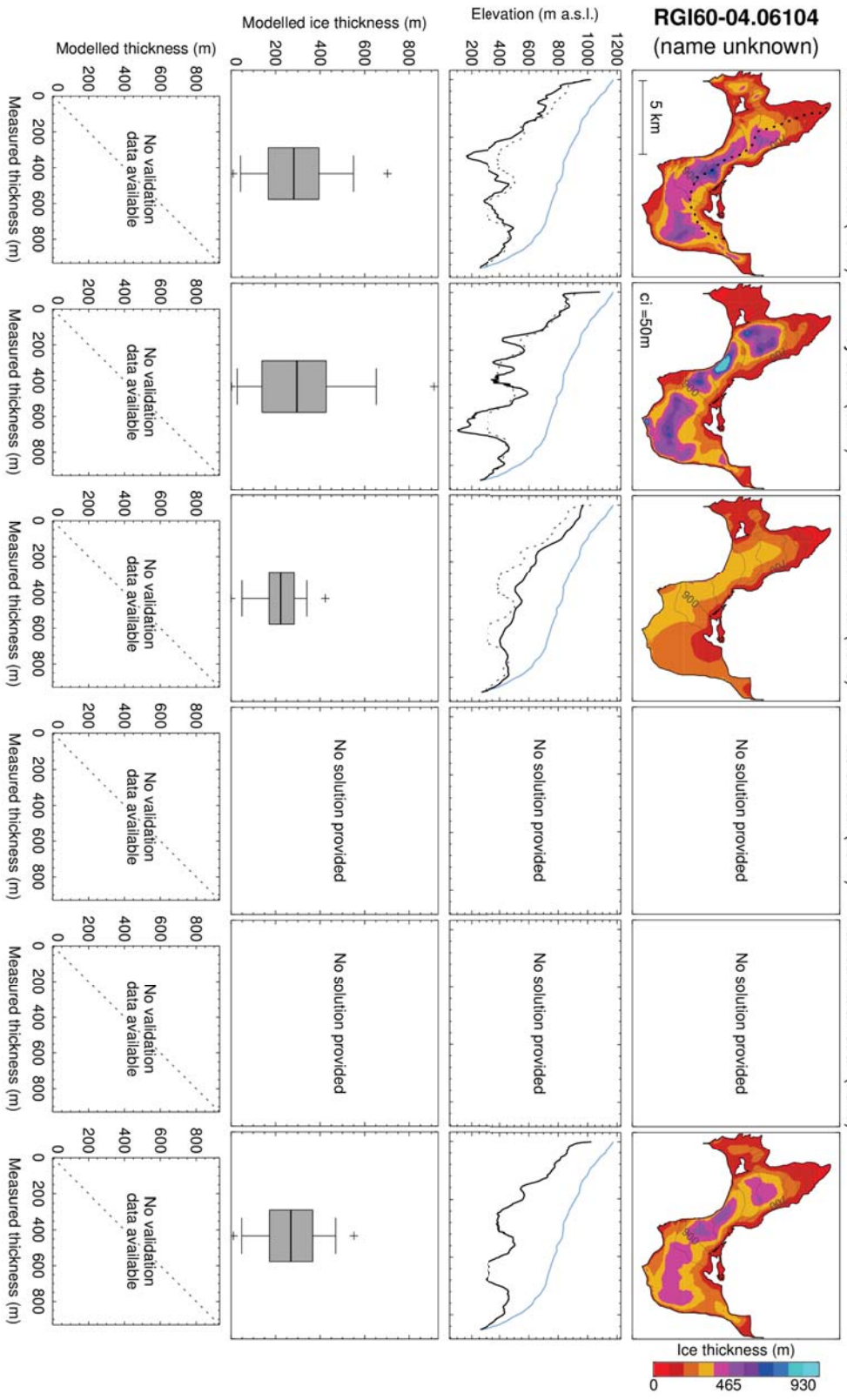


Figure S 10: Same as Figure S 7 but for glacier RGI60-04.06104 (RGI region "Arctic Canada South").

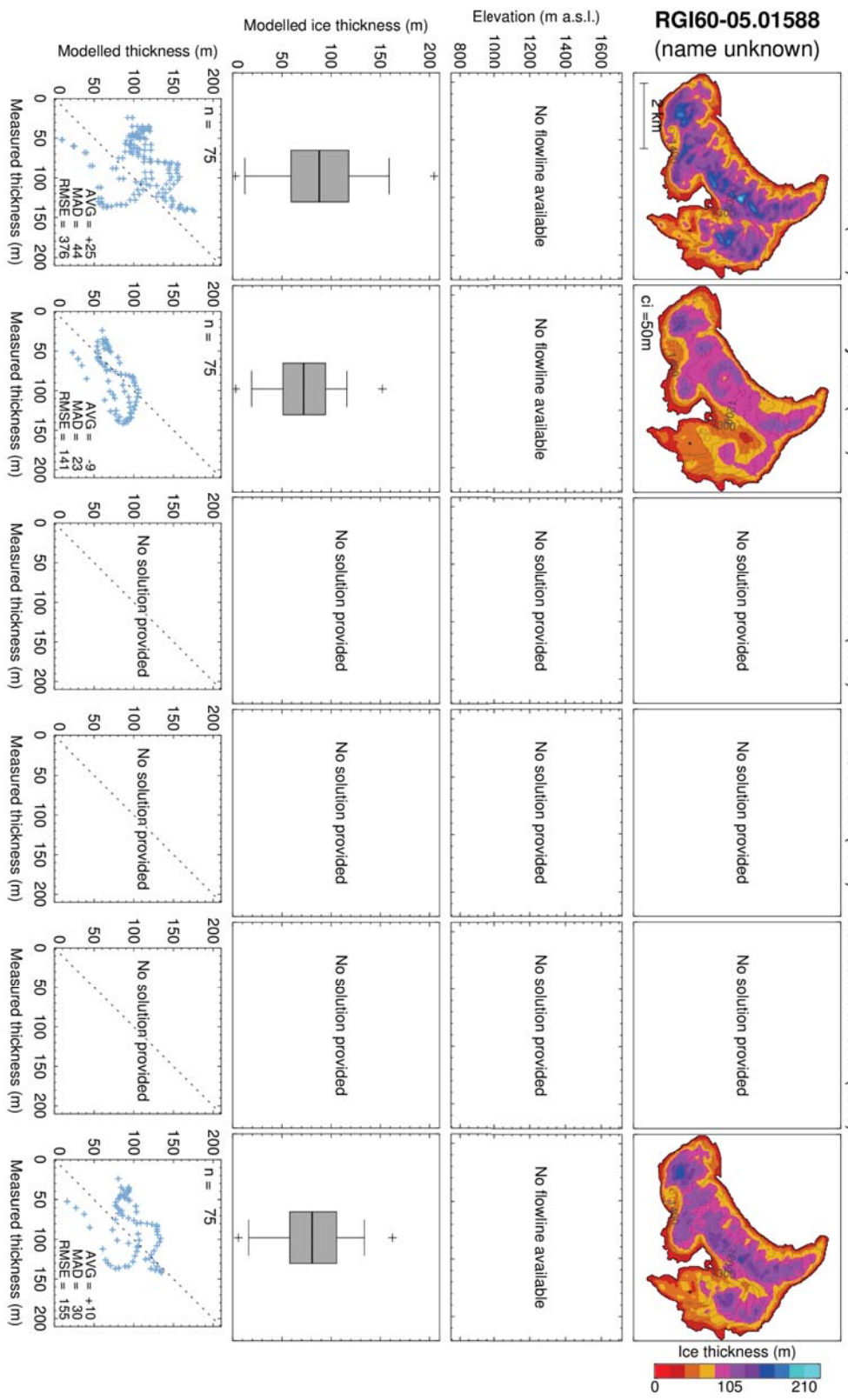


Figure S 11: Same as Figure S 7 but for glacier RGI60-05.01588 (RGI region "Greenland Periphery").

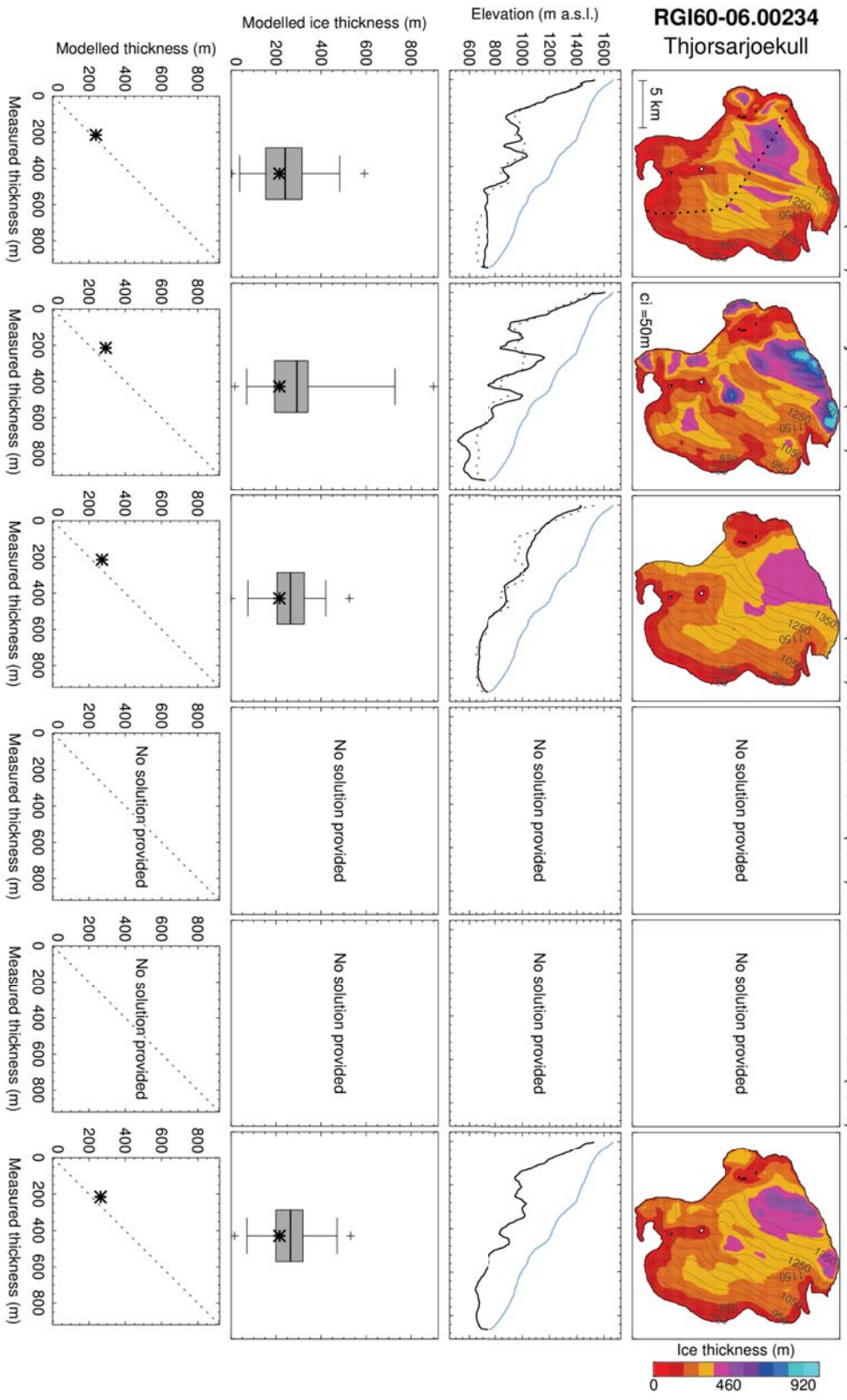


Figure S 12: Same as Figure S 7 but for glacier RGI60-06.00234 (RGI region "Iceland").

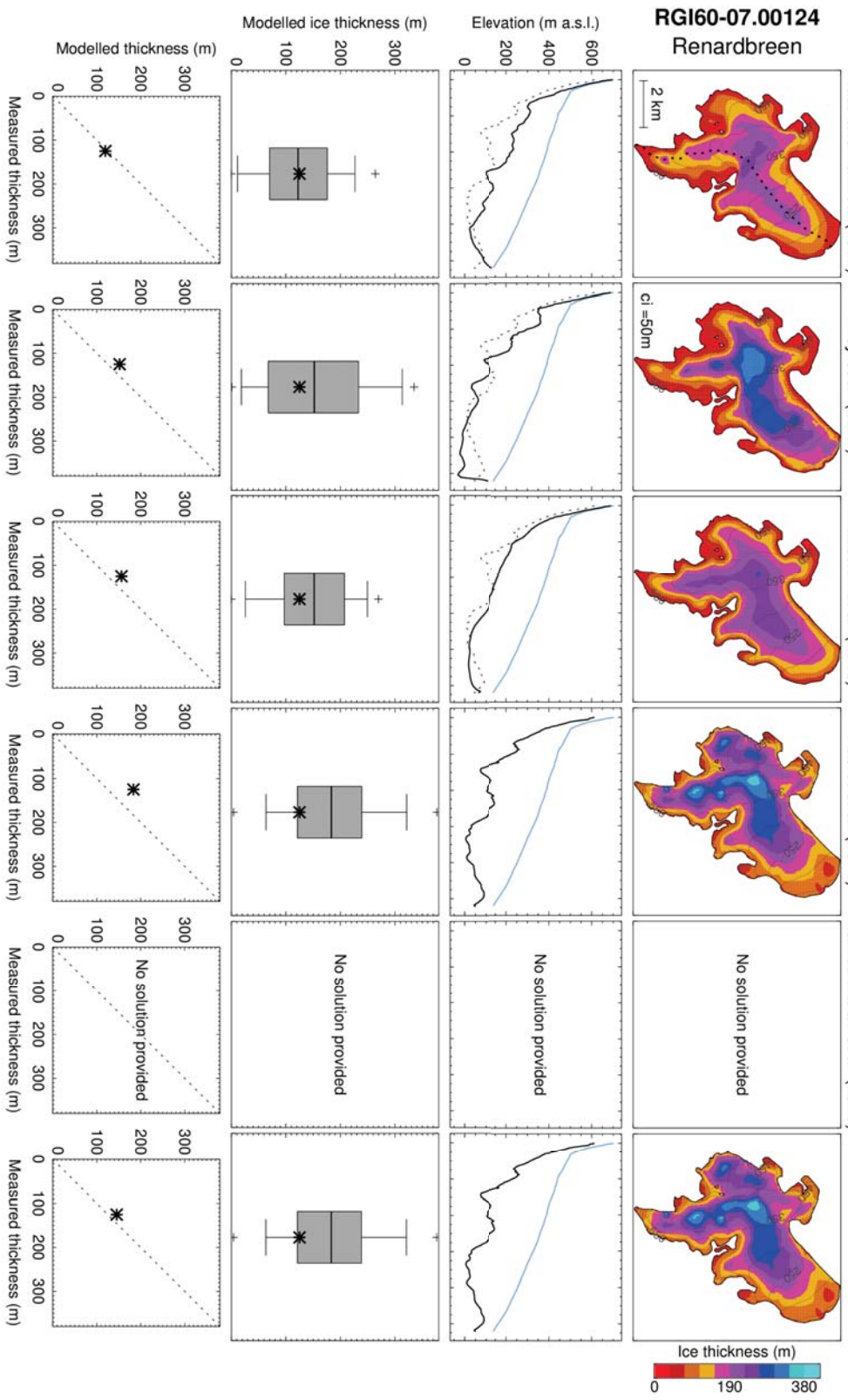


Figure S 13: Same as Figure S 7 but for glacier RGI60-07.00124 (RGI region "Svalbard").

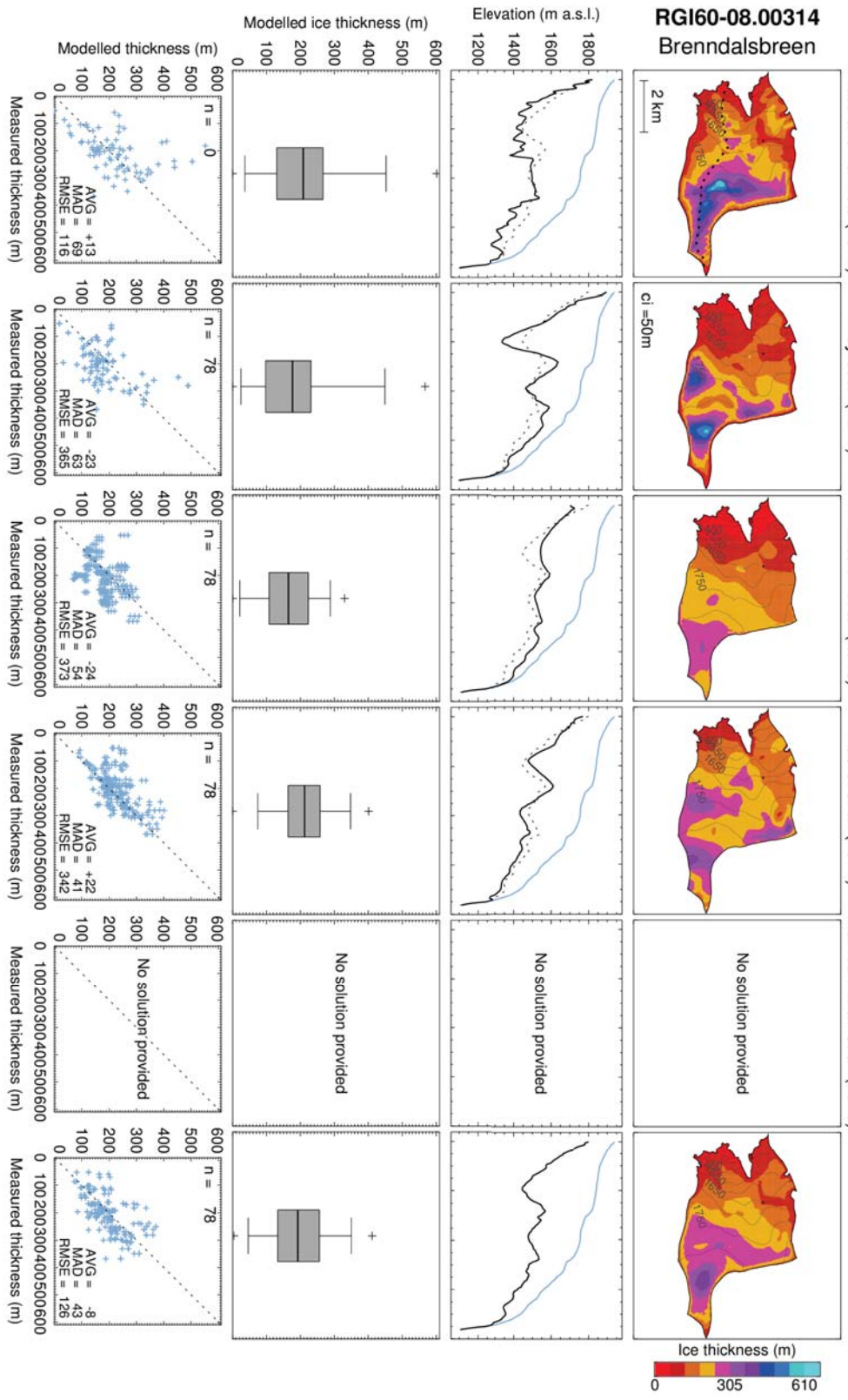


Figure S 14: Same as Figure S 7 but for glacier RGI60-08.00314 (RGI region "Scandinavia").

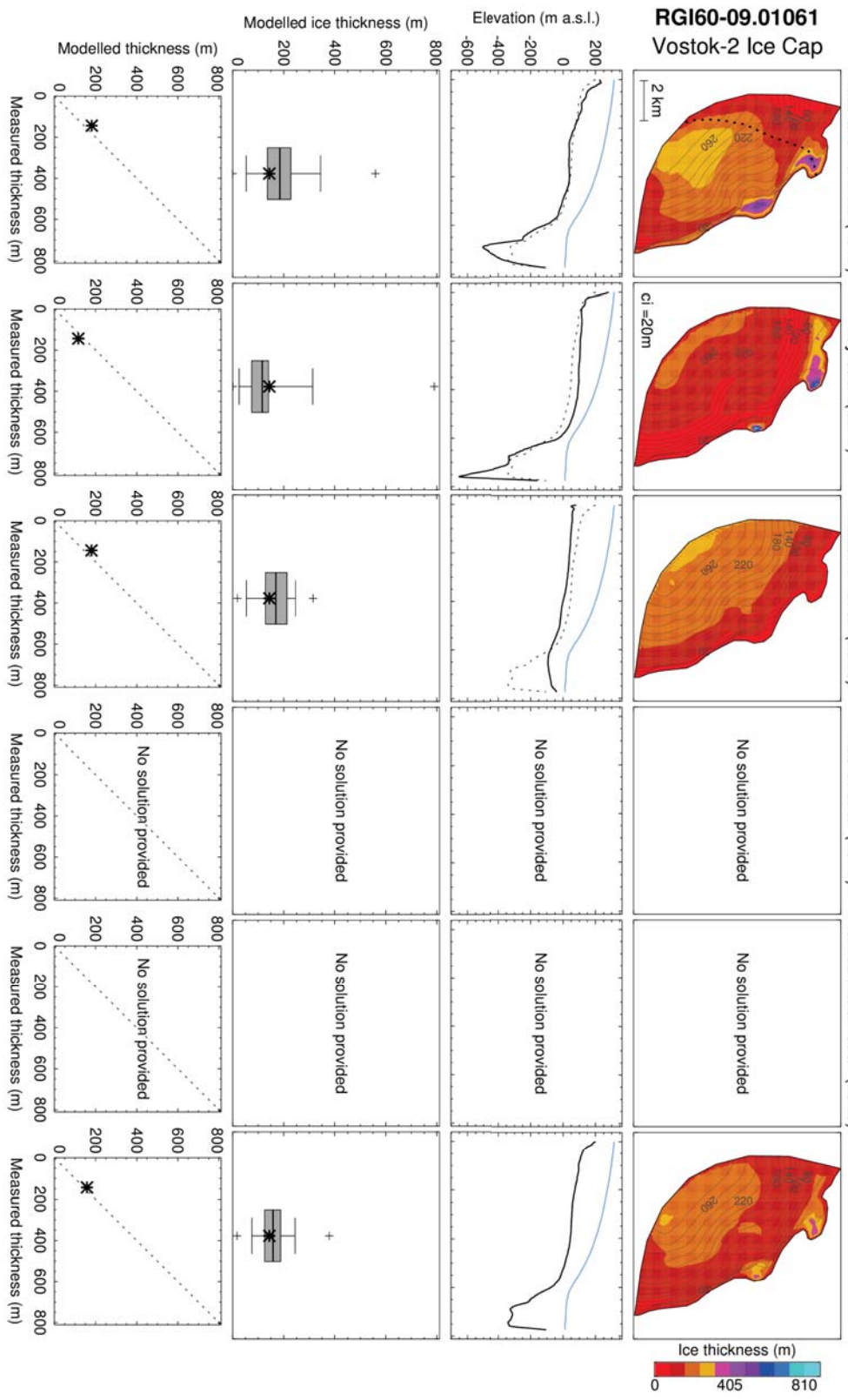


Figure S 15: Same as Figure S 7 but for glacier RGI60-09.01061 (RGI region "Russian Arctic").

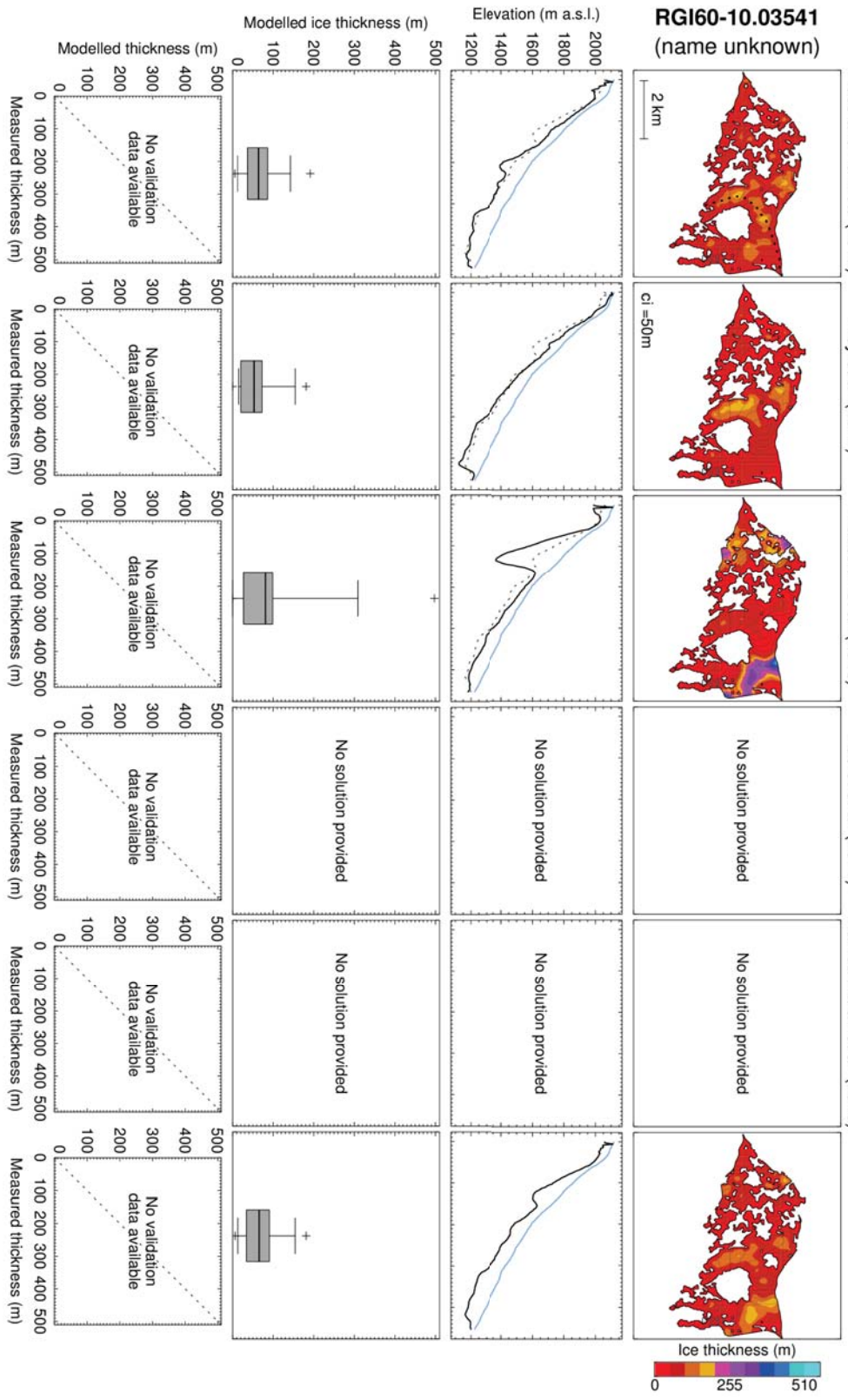


Figure S 16: Same as Figure S 7 but for glacier RGI60-10.03541 (RGI region "North Asia").

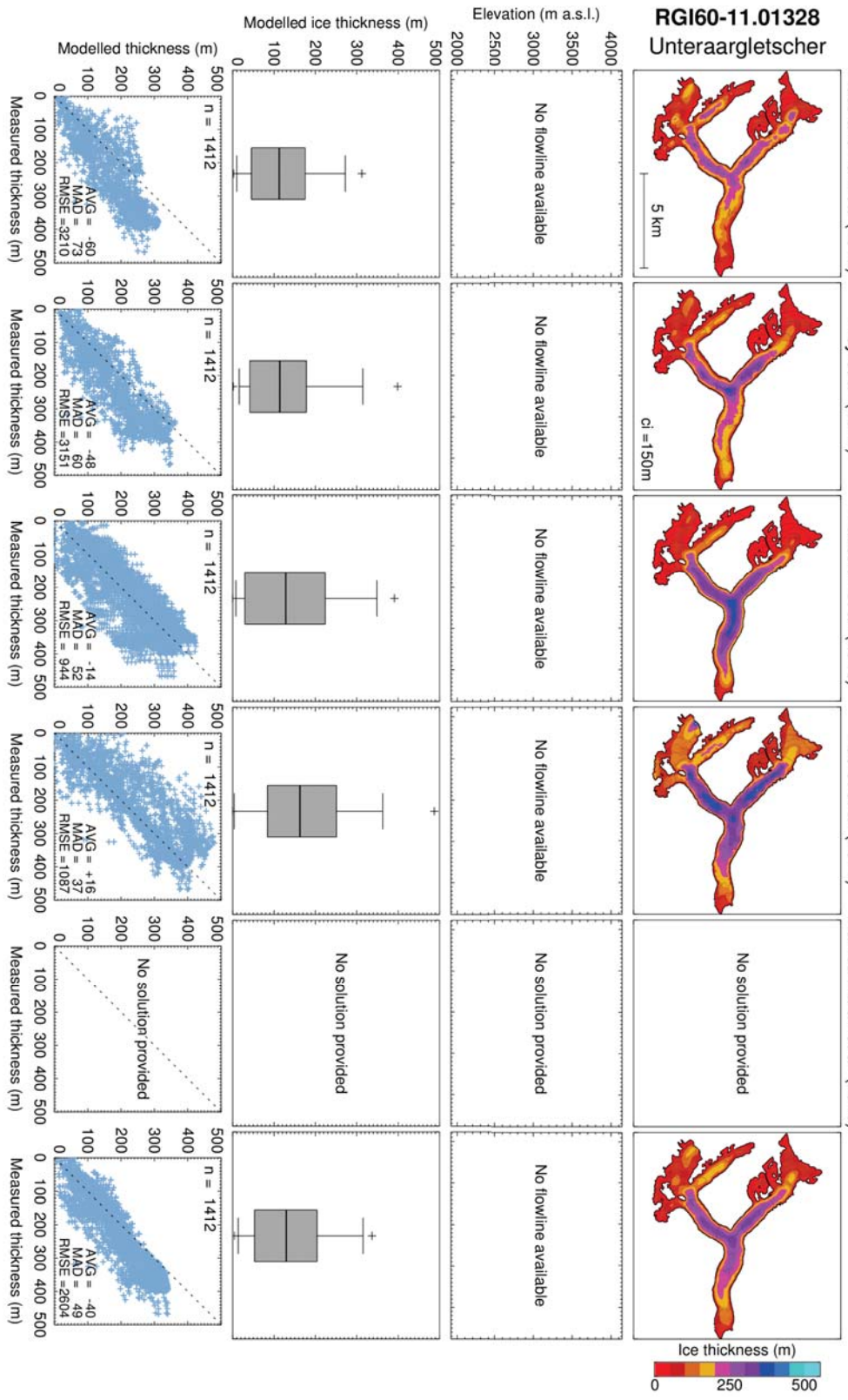


Figure S 17: Same as Figure S 7 but for glacier RGI60-11.01328 (RGI region "Central Europe").

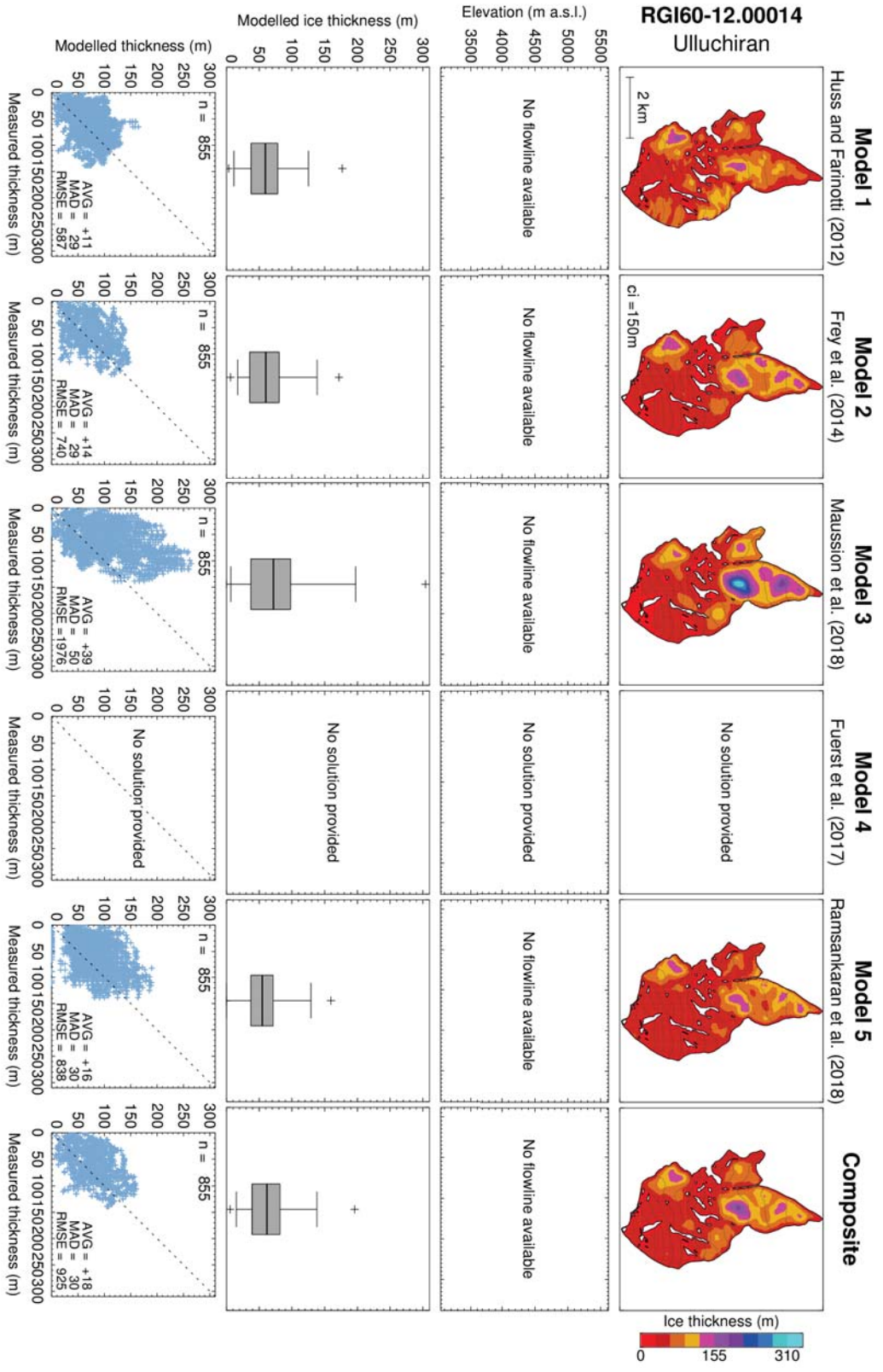


Figure S 18: Same as Figure S 7 but for glacier RGI60-12.00014 (RGI region "Caucasus and Middle East").

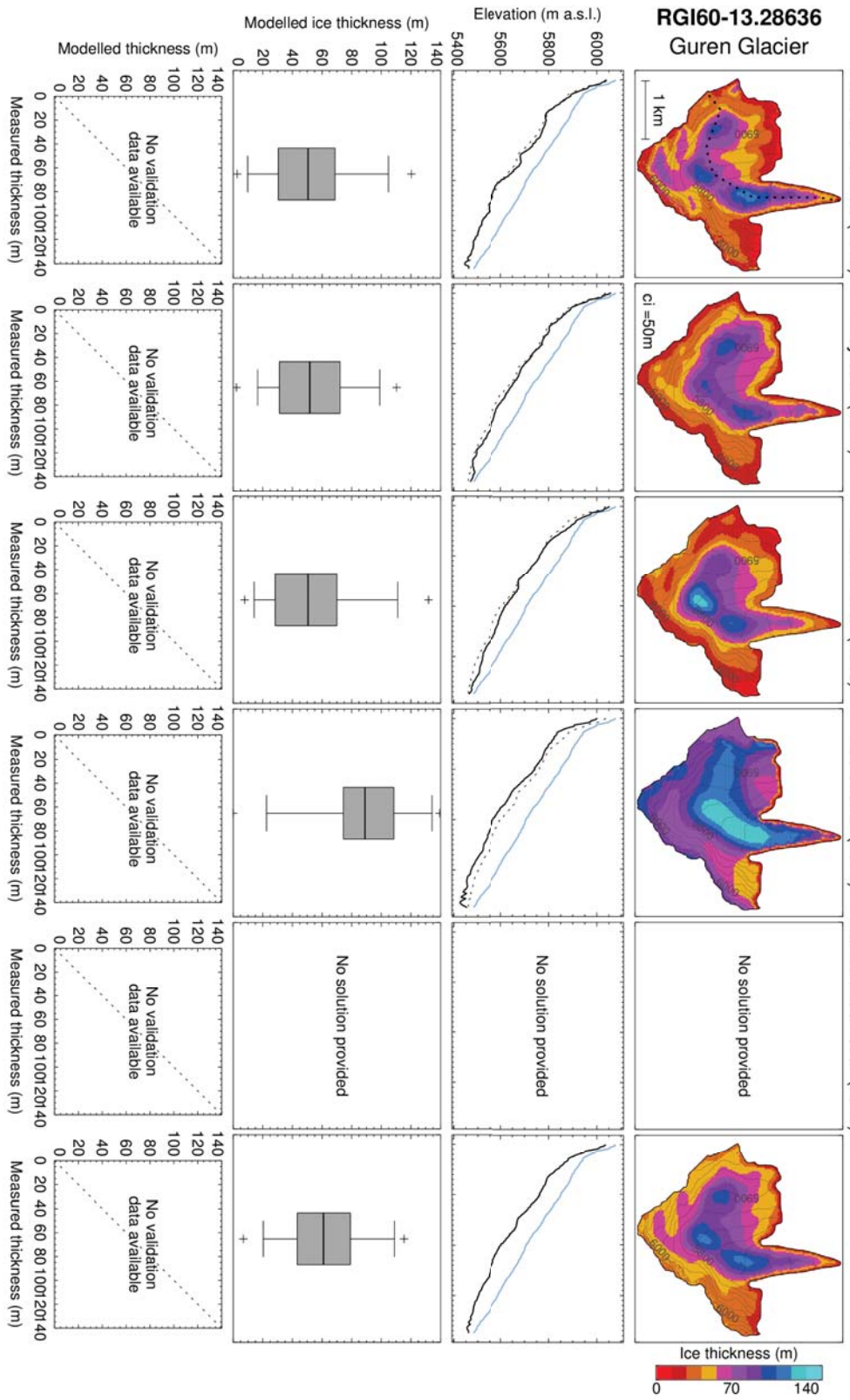


Figure S 19: Same as Figure S 7 but for glacier RGI60-13.28636 (RGI region "Central Asia").

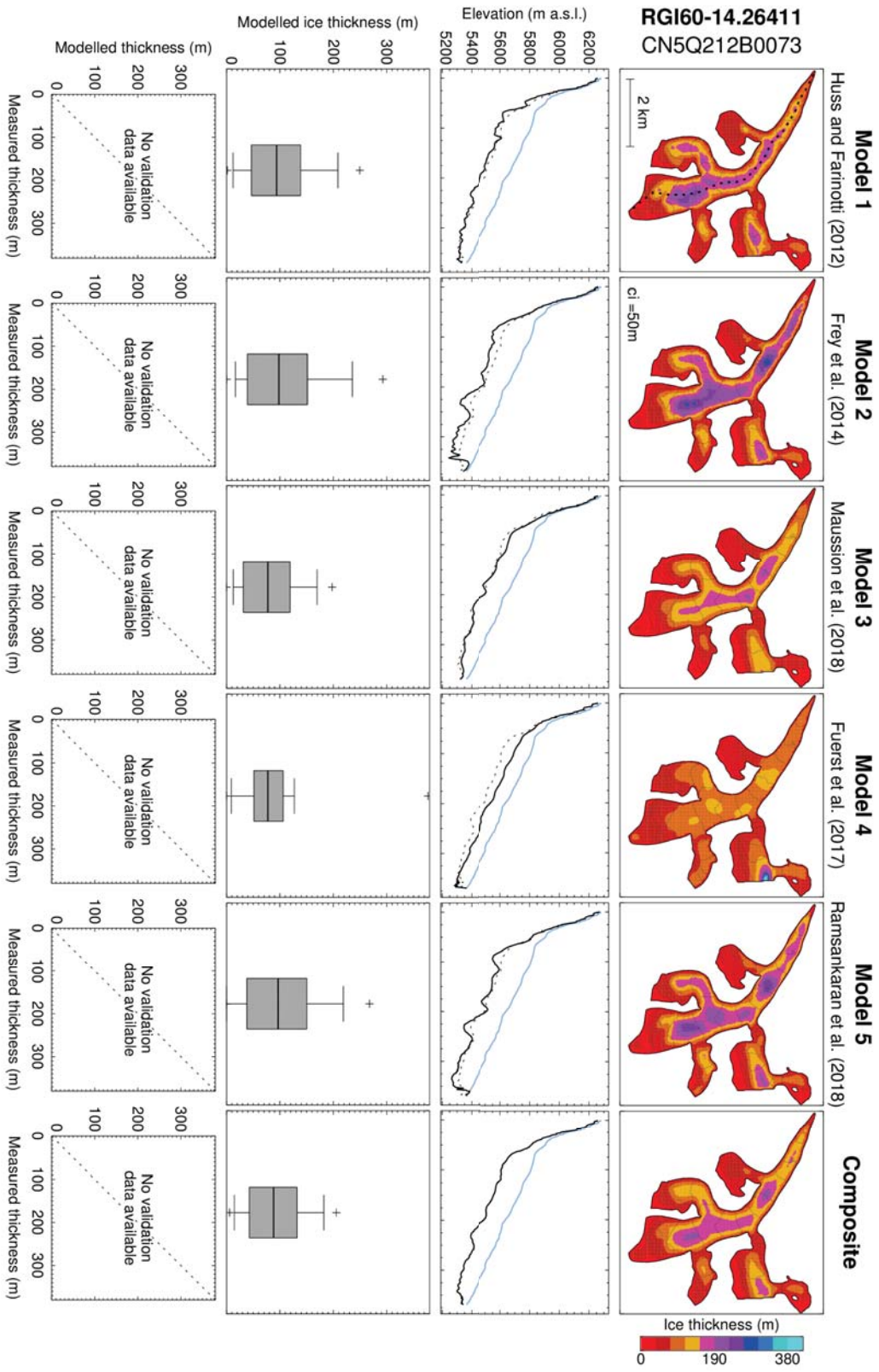


Figure S 20: Same as Figure S 7 but for glacier RGI60-14.26411 (RGI region "South Asia West").

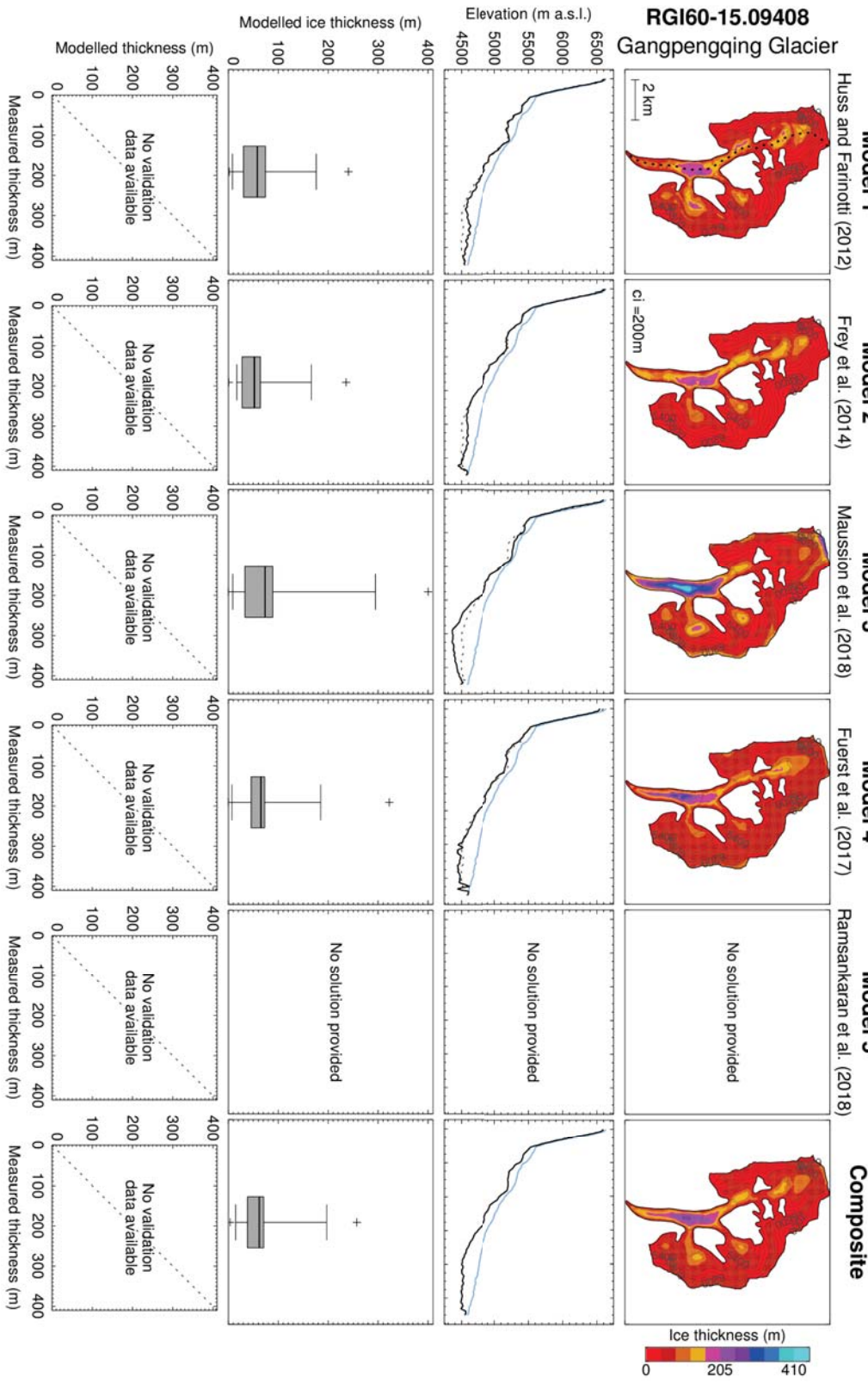


Figure S 21: Same as Figure S 7 but for glacier RGI60-15.09408 (RGI region "South Asia East").

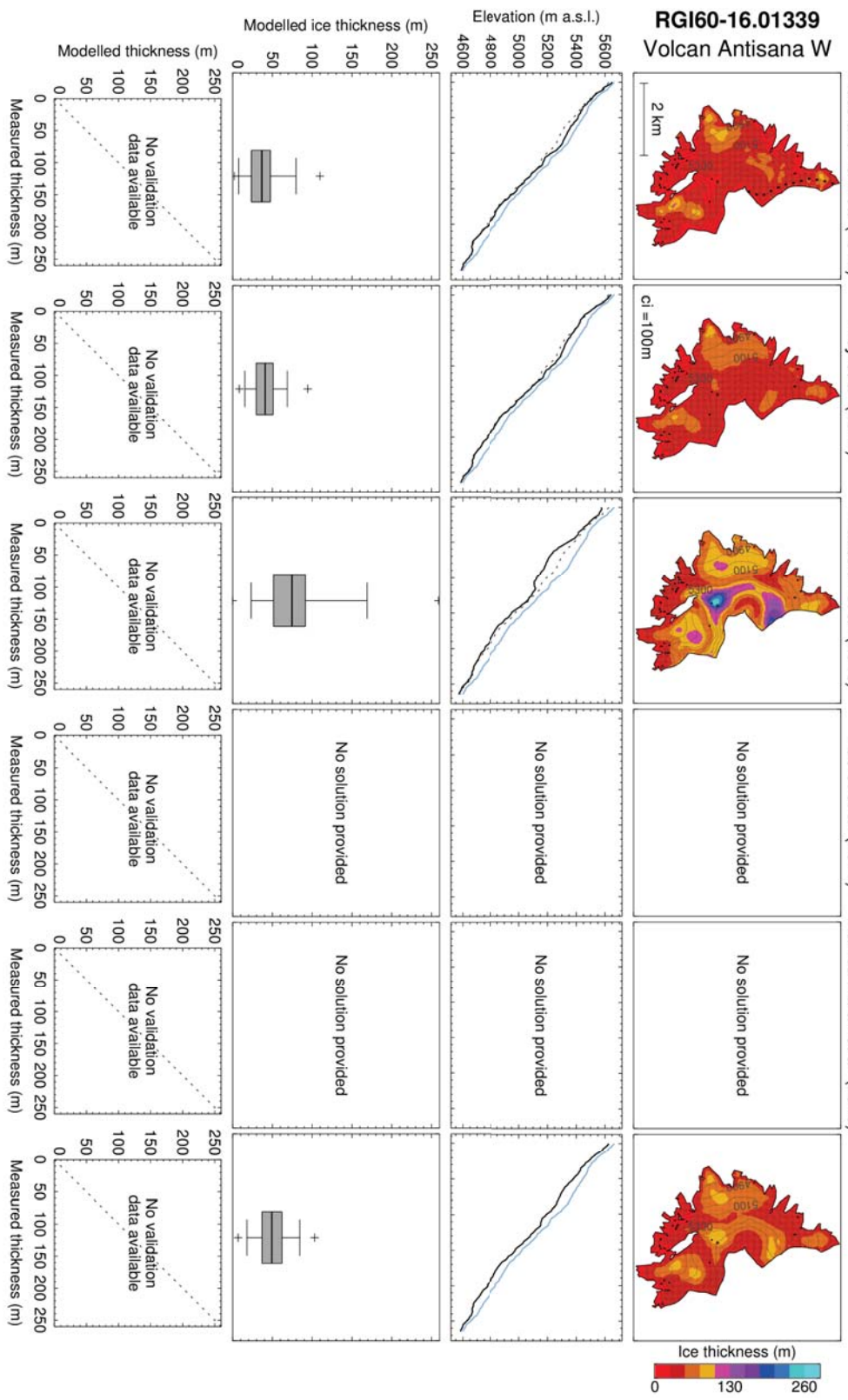


Figure S 22: Same as Figure S 7 but for glacier RGI60-16.01339 (RGI region "Low Latitudes").

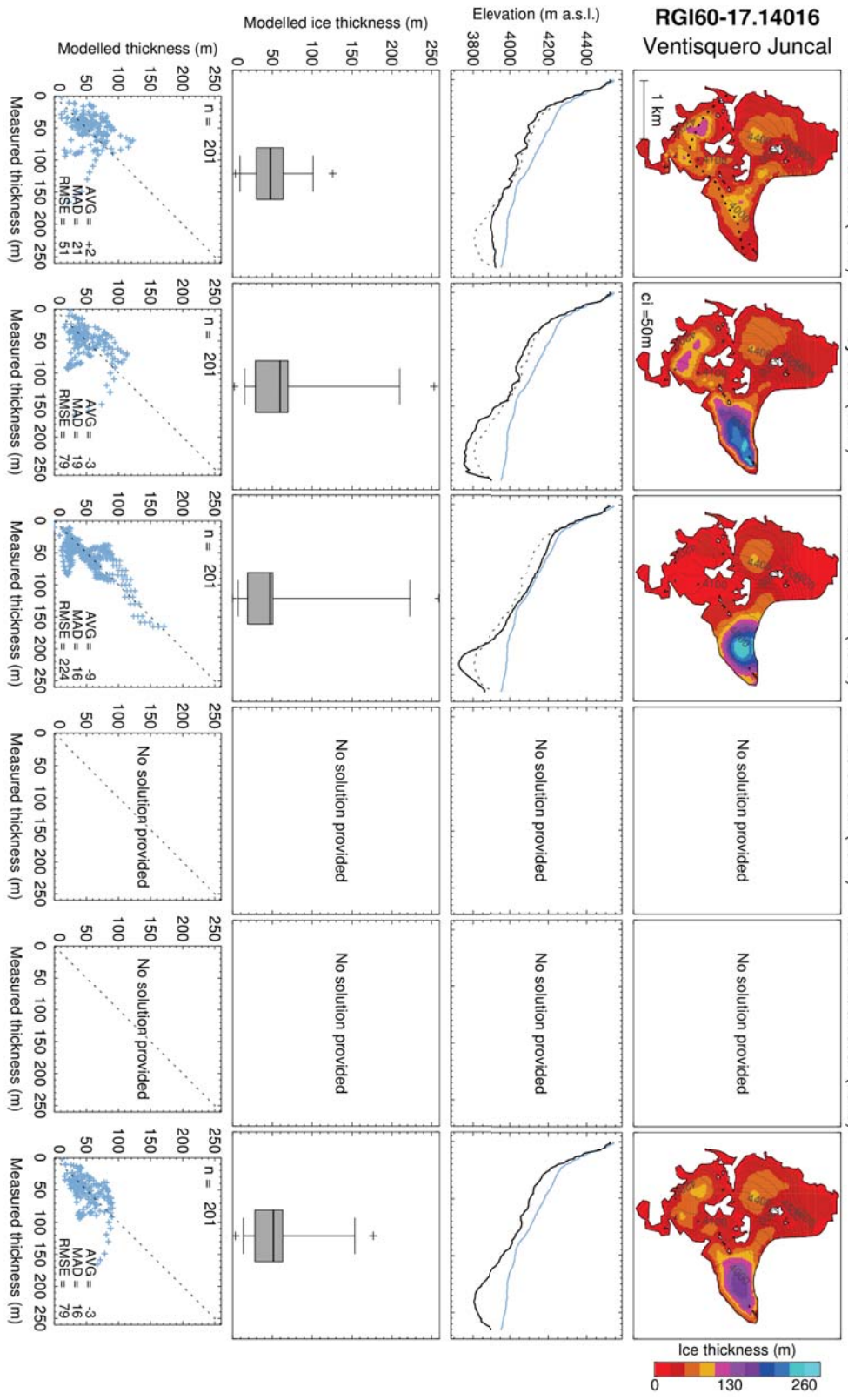


Figure S 23: Same as Figure S 7 but for glacier RGI60-17.14016 (RGI region "Southern Andes").

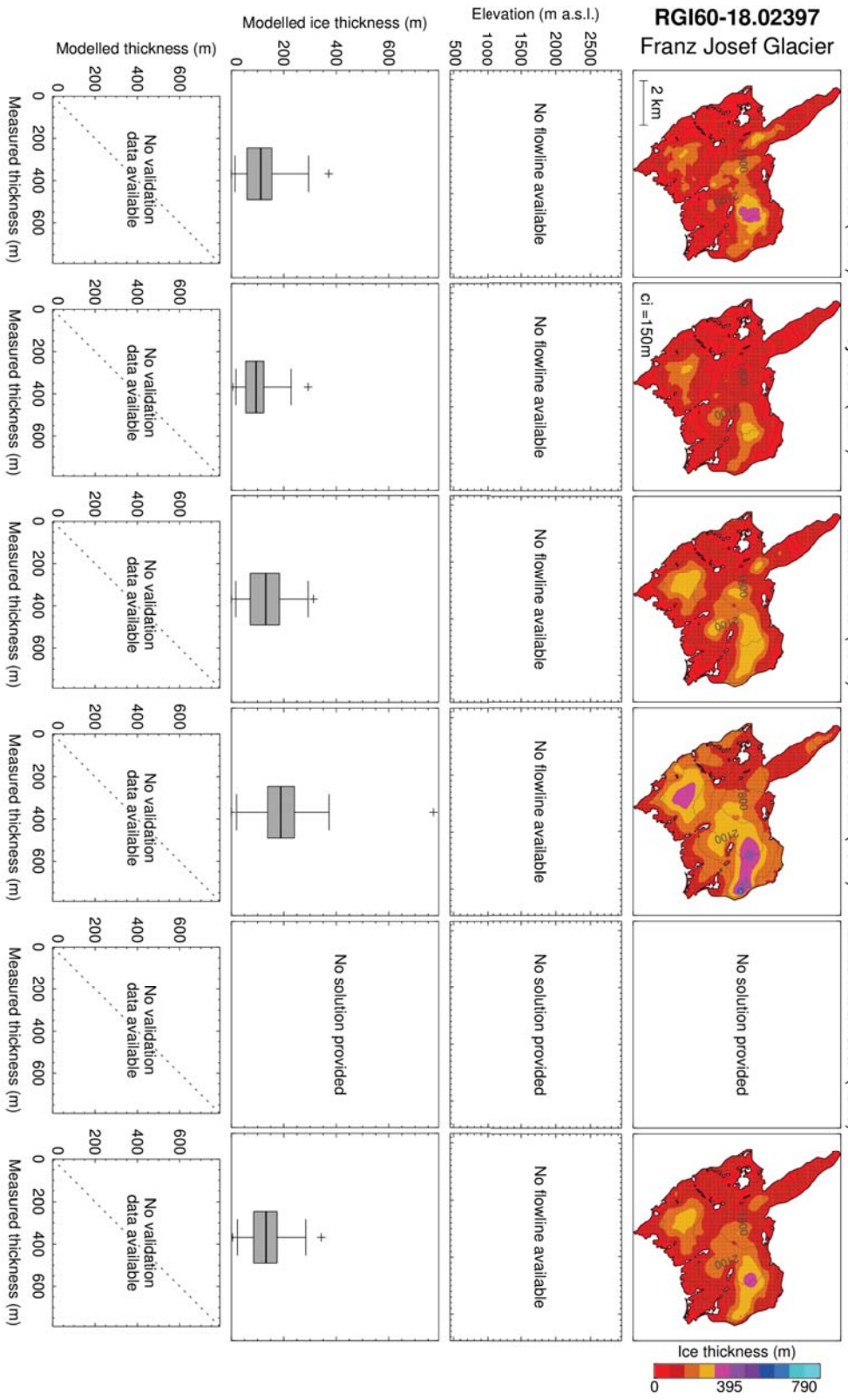


Figure S 24: Same as Figure S 7 but for glacier RGI60-18.02397 (RGI region "New Zealand").

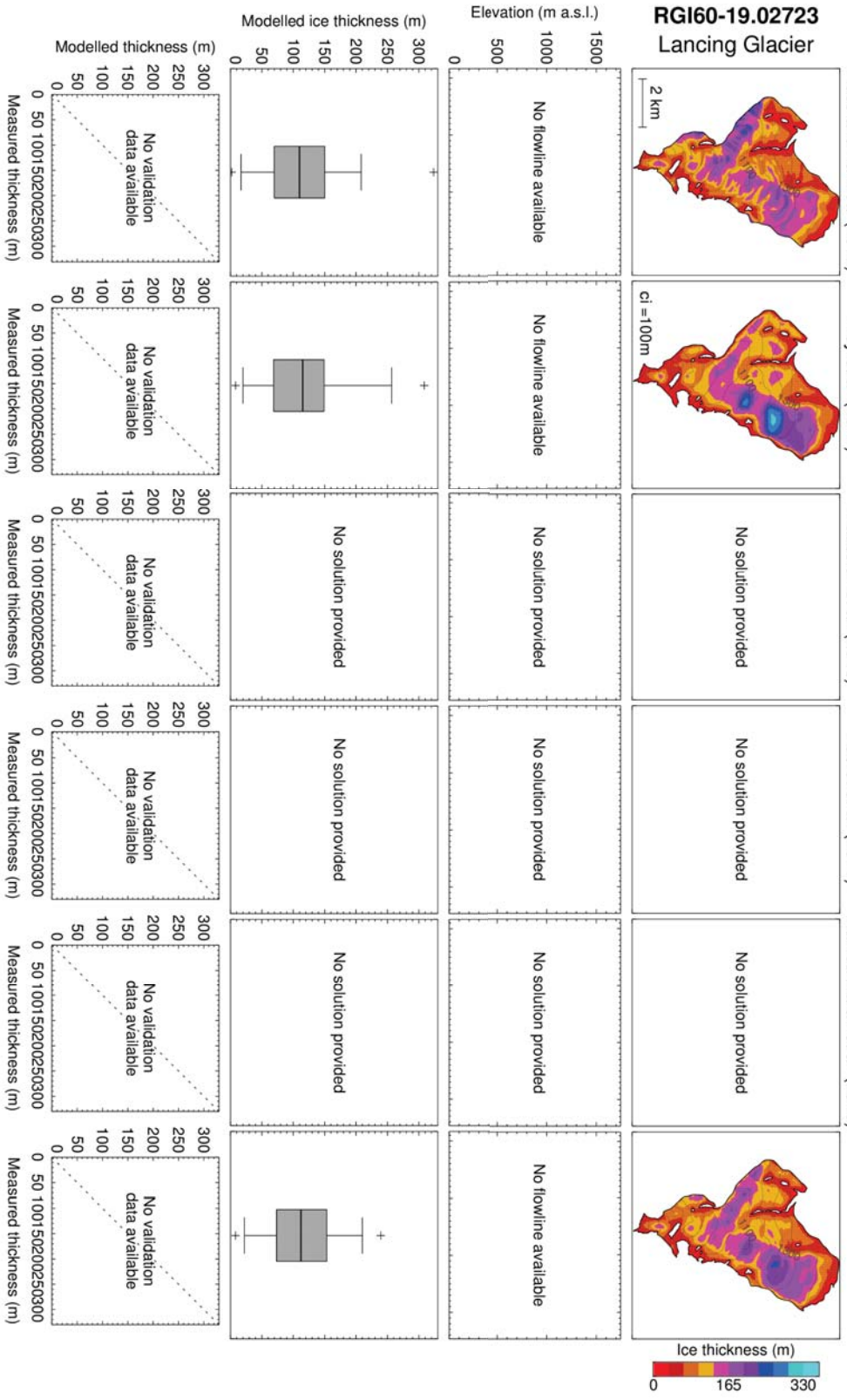


Figure S 25: Same as Figure S 7 but for glacier RGI60-19.02723 (RGI region "Antarctic and Subantarctic").

# Supplementary References


Farinotti, D., Brinkerhoff, D. J., Clarke, G. K. C., Fürst, J. J., Frey, H., Gantayat, P., Gillet-Chaulet, F., Girard, C., Huss, M., Leclercq, P. W., Linsbauer, A., Machguth, H., Martin, C., Maussion, F., Morlighem, M., Mosbeux, C., Pandit, A., Portmann, A., Rabatel, A., Ramsankaran, R., Reerink, T. J., Sanchez, O., Stentoft, P. A., Singh Kumari, S., van Pelt, W. J. J., Anderson, B., Benham, T., Binder, D., Dowdeswell, J. A., Fischer, A., Helfricht, K., Kutuzov, S., Lavrentiev, I., McNabb, R., Gudmundsson, G. H., Li, H., and Andreassen, L. M. (2017). How accurate are estimates of glacier ice thickness? Results from ITMIX, the Ice Thickness Models Intercomparison eXperiment. *The Cryosphere*, 11(2):949–970.

Farinotti, D., Huss, M., Bauder, A., Funk, M., and Truffer, M. (2009). A method to estimate ice volume and ice thickness distribution of alpine glaciers. *Journal of Glaciology*, 55(191):422–430.

Frey, H., Machguth, H., Huss, M., Huggel, C., Bajracharya, S., Bolch, T., Kulkarni, A., Linsbauer, A., Salzmann, N., and Stoffel, M. (2014). Estimating the volume of glaciers in the Himalayan–Karakoram region using different methods. *The Cryosphere*, 8(6):2313–2333.

Fürst, J., Navarro, F., Gillet-Chaulet, F., M., H., Moholdt, G., Fettweis, X., Lang, C., Seehaus, T., Ai, S., Benham, T., Benn, D., Björnsson, H., Dowdeswell, J., Grabiec, M., Kohler, J., Lavrentiev, I., Lindbäck, K., Melvold, K., Pettersson, R., Rippin, D., Saintenoy, A., Sánchez-Gámez, P., Schuler, T., Sevestre, H., Vasilenko, E., and Braun, M. (2018). The ice-free topography of Svalbard. *Geophysical Research Letters*.

Fürst, J. J., Gillet-Chaulet, F., Benham, T. J., Dowdeswell, J. A., Grabiec, M., Navarro, F., Pettersson, R., Moholdt, G., Nuth, C., Sass, B., Aas, K., Fettweis, X., Lang, C., Seehaus, T., and Braun, M. (2017). Application of a two-step approach for mapping ice thickness to various glacier types on Svalbard. *The Cryosphere*, 11(5):2003–2032.

Glen, J. W. (1955). The creep of polycrystalline ice. *Proceedings of the Royal Society of London, Series A*, 228(1175):519–538.

Grinsted, A. (2013). An estimate of global glacier volume. *The Cryosphere*, 7:141–151.

Haeberli, W. and Hoelzle, M. (1995). Application of inventory data for estimating characteristics of and regional climate-change effects on mountain glaciers: a pilot study with the European Alps. *Annals of Glaciology*, 21:206–212.

Harris, I., Jones, P. D., Osborn, T. J., and Lister, D. H. (2014). Updated high-resolution grids of monthly climatic observations the CRU TS3.10 Dataset. *International Journal of Climatology*, 34(3):623–642.

Huss, M. and Farinotti, D. (2012). Distributed ice thickness and volume of all glaciers around the globe. *Journal of Geophysical Research*, 117:F04010.

Huss, M. and Hock, R. (2015). A new model for global glacier change and sea-level rise. *Frontiers in Earth Science*, 3:Art. 54.

Huss, M., Jouvet, G., Farinotti, D., and Bauder, A. (2010). Future high-mountain hydrology: a new parameterization of glacier retreat. *Hydrology and Earth System Sciences*, 14:815–829.

Kienholz, C., Rich, J. L., Arendt, A. A., and Hock, R. (2014). A new method for deriving glacier centerlines applied to glaciers in Alaska and northwest Canada. *The Cryosphere*, 8(2):503–519.

Linsbauer, A., Paul, F., and Haeberli, W. (2012). Modeling glacier thickness distribution and bed topography over entire mountain ranges with GlabTop: Application of a fast and robust approach. *Journal of Geophysical Research*, 117:F03007.

Martín-Español, A., Navarro, F., Otero, J., Lapazaran, J., and Blaszczyk, M. (2015). Estimate of the total volume of Svalbard glaciers, and their potential contribution to sea-level rise, using new regionally based scaling relationships. *Journal of Glaciology*, 61(225):2941.

Marzeion, B., Jarosch, A., and Hofer, M. (2012). Past and future sea-level change from the surface mass balance of glaciers. *The Cryosphere*, 6:1295–1322.

Maussion, F., Butenko, A., Eis, J., Fourteau, K., Jarosch, A. H., Landmann, J., Oesterle, F., Recinos, B., Rothenpieler, T., Vlug, A., Wild, C. T., and Marzeion, B. (2018). The Open Global Glacier Model (OGGM) v1.0. *Geoscientific Model Development Discussions*, 2018:1–33.

Meinshausen, M., Smith, S., Calvin, K., Daniel, J., Kainuma, M., Lamarque, J.-F., Matsumoto, K., Montzka, S., Raper, S., Riahi, K., Thomson, A., Velders, G., and van Vuuren, D. (2011). The RCP greenhouse gas concentrations and their extensions from 1765 to 2300. *Climatic Change*, 109(1-2):213–241.

Paterson, W. S. B. (1994). *The Physics of Glaciers*. Pergamon, New York, third edition.

Radić, V., Bliss, A., Beedlow, A., Hock, R., Miles, E., and Cogley, J. (2014). Regional and global projections of twenty-first century glacier mass changes in response to climate scenarios from global climate models. *Climate Dynamics*, pages 1–22.

Radić, V. and Hock, R. (2010). Regional and global volumes of glaciers derived from statistical upscaling of glacier inventory data. *Journal of Geophysical Research*, 115:F01010.

Ramsankaran, R., Pandit, A., and Azam, M. (2018). Spatially distributed ice-thickness modelling for Chhota Shigri Glacier in western Himalayas, India. *International Journal of Remote Sensing*, 39(10):3320–3343.

WGMS (2016). Glacier thickness database 2.0. I. Gärtner-Roer, L. M. Andreassen, E. Bjerre, D. Farinotti, A. Fischer, M. Fischer, K. Helfricht, M. Huss, T. Knecht, S. Kutuzov, J. Landmann,I. Lavrentiev, H. Li, Z. Li, H. Machguth, K. Naegeli, F. Navarro, A. Rabatel, P. Stentoft, M. Zemp (eds.), World Glacier Monitoring Service, Zurich, Switzerland.